IEEE Access
Multidisciplinary | Rapid Review | Open Access Journal

Received September 4, 2020, accepted September 11, 2020, date of publication September 18, 2020,
date of current version September 29, 2020.

Digital Object Identifier 10.1109/ACCESS.2020.3024830

Improving the Cross-Border Activation of the Regulating Reserve to Enhance the Provision of Load-Frequency Control

MARCEL TOPLER, (Graduate Student Member, IEEE), JOŽEF RITONJA, (Member, IEEE), AND BOŠTJAN POLAJŽER, (Member, IEEE)
Faculty of Electrical Engineering and Computer Science, University of Maribor, 2000 Maribor, Slovenia
Corresponding author: Marcel Topler (marcel.topler@um.si)

This work was supported by the Slovenian Research Agency (ARRS) under Project P2-0115 and Project L2-7556.

ABSTRACT This paper presents the Cross-Border activation of the Regulating Reserve (CBRR) between participating Control Areas (CAs), which is being developed to reduce the costs of balancing energy. The main objective of the CBRR is to activate the regulating reserve in participating CAs, to release the regulating reserve and to reduce the balancing energy as part of the safe operation of the power system. However, the classic CBRR includes a frequency term and, therefore, inherently affects the frequency response of the participating CAs, which is not discussed in the literature. In this paper, the impact of the classic CBRR on frequency quality and the provision of Load-Frequency Control (LFC) is thoroughly evaluated with dynamic simulations of a three-CA test system and an eigenvalue analysis of a two-CA system. It is clearly demonstrated that the classic CBRR reduces the damping of the entire power system. Therefore, a modified implementation of the classic CBRR is presented, and a modified CBRR is proposed, which has no impact on the system's eigendynamics. Furthermore, the results of the dynamic simulations confirm that the frequency quality can be improved by the classic CBRR, although there are also cases where it can deteriorate. However, the modified CBRR improves the frequency quality in all cases. The modified CBRR also improves the indicators for the provision of LFC compared to the classic CBRR. Moreover, the modified CBRR reduces the unintended exchange of energy and the demand power, thus increasing the financial effects of the CBRR's activation.

INDEX TERMS Balancing energy, cross-border activation, eigenvalue analysis, Load-Frequency Control, regulating reserve.

NOMENCLATURE

N	Number of participating CAs.
ACE'_i, ACE_i, ACE^*_i	Area Control Error for LFC, CBRR and modified CBRR of the i-th CA.
B_i	Frequency-bias coefficient of the i-th CA.
$\Delta f_i, f_{ai}, f_{si}$	Frequency deviation, actual and scheduled freqeuency of the i-th CA.
$\Delta P_i, P_{ai}, P_{si}$	Interchange power variation, actual and scheduled interchange power of the i-th CA.
ΔP_{ei}	Actual (electrical) control power of the i-th CA.
ΔP_{sci}	Scheduled control power of the i-th CA.
ΔP_{Li}	Load-power variation of the i-th CA.
K_i	CBRR activation factor of the i-th CA.
P_{di}, P_{di^*}	Demand power for CBRR and modified CBRR of the i-th CA.
P_{cori}, P^*_{cori}	Correction power for CBRR and modified CBRR of the i-th CA.
$\mathbf{x}, \mathbf{A}$	State vector and matrix.
$\mathbf{u}, \mathbf{B}$	Input vector and matrix.
λ^n	Eigenvalue of $\mathbf{A}$.
a_n	Coefficient of a characteristic polynomial.
H_i	Inertia time constant of the i-th CA.
D_i	Damping coefficent of the i-th CA.

The associate editor coordinating the review of this manuscript and approving it for publication was Ziang Zhang.

$T_{\mathrm{CH}i}$	Time constant of the main inlet volume and steam chest of the i-th CA.
$F_{\mathrm{HP}i}$	A fraction of the total turbine power generated by the high-pressure turbine section of the i-th CA.
$T_{\mathrm{RH}i}$, $T_{\mathrm{R}i}$, $T_{\mathrm{W}i}$	Time constant of the re-heater, reset time and water start time of the i-th CA.
$R_{\mathrm{T}i}$, $R_{\mathrm{P}i}$	Temporary droop and permanent droop of the i-th CA.
$\alpha_{\mathrm{k}i}$	Participation factor of the k-th control unit in the i-th CA.
$R_{\mathrm{k}i}$	Droop characteristic of the k-th control unit in the i-th CA.
$K_{\mathrm{r}i}$, $T_{\mathrm{r}i}$	Gain and time constant of PI controller of the i-th CA.
$T_{\mathrm{LPF}i}$, $T_{\mathrm{G}i}$	Time constant of a Low-Pass Filter and governor time constant of the i-th CA.
T_{ij}	Tie-line parameter between the i-th and j-th CA.
$z(t)$, $w(t)$	State variable and Gaussian white noise used for the random load model.
σ_L, μ_L, ρ_L	Standard deviation, mean value and auto-correlation of the random load.
$\sigma_{\Delta f_i}$, σ_{ACE_i}	Standard deviations of the variables Δf_i and ACE_i of the i-th CA.
$\mu_{\mathrm{RoCoF}_{i+}}$, $\mu_{\mathrm{RoCoF}_{i-}}$	Mean values of positive and negative values of RoCoF of the i-th CA.
$\Delta W_{\mathrm{un}i+}$, $\Delta W_{\mathrm{un}i-}$	Positive and negative unintended exchange of energy of the i-th CA.
$P_{\mathrm{d}i+}$, $P_{\mathrm{d}i-}$	Positive and negative demand power of the i-th CA.

I. INTRODUCTION

A. MOTIVATION AND LITERATURE REVIEW

Interconnections between neighboring Control Areas (CAs) have become a global trend in the development of power systems to increase the stability of the power system and to achieve a variety of economic benefits [1]. As a result, Transmission System Operators (TSOs) face new challenges in the operation of power systems because of the increased cross-border energy trade, the development of ancillary-services markets, increased penetration of renewable-energy sources and the reduction in the cost of operating the power system [2]–[7]. Therefore, advanced control techniques and methods are continually being developed to enhance the reliability, security, and efficiency of power supplies in future power systems [8]. In the first quarter of 2020, the development of the Cross-Border Activation of the Regulating Reserve (CBRR) began, which is to be implemented in continental Europe by the members of the European Network of Transmission System Operators for Electricity (ENTSO-E) in the third quarter of 2022 [9]. The CBRR aims to activate the regulating reserve in participating CAs and reduce the balancing energy [10]. As a result, the associated financial costs can be reduced. However, several questions need to be answered regarding the impact of the CBRR on the power system's dynamics and the provision of Load-Frequency Control (LFC), mainly because the quality of the frequency is declining [11].

The frequency of a power system depends on the balance between the generation and consumption of electrical energy. A change in the active-power demand at one point of a power system is reflected throughout the system in a frequency deviation [12]. Maintaining frequency and power interchanges with CAs at the scheduled values are the two main objectives of a power system's LFC [13], which is one of the functionalities of Automatic Generation Control (AGC) [14]. TSOs are therefore obliged to maintain the balance between generation and consumption in their CA by activating regulating reserves. Grid Control Cooperation (GCC) was introduced in Europe [15] to avoid the counter-activation of regulating reserves in participating CAs. The Imbalance Netting Process (INP) was implemented with the involvement of four German TSOs in 2008 [16]. The activation of the regulating reserve is thus reduced in addition to the reduced financial costs [17]. Shortly after that, international extensions were made, and the GCC developed into the International GCC (IGCC) [18], [19].

However, the further development of the INP is necessary due to new network codes and the increasing demand for cost optimization, which must be implemented so that the CBRR will be enabled [9]. CAs with the same sign of demand power will be able to activate the demand for balancing energy in participating CAs [10]. The TSOs agreed to use the control-demand approach for the CBRR, which is the same approach as currently used for the INP. The main objective of the design, implementation, and operation of the CBRR is to integrate the markets for balancing services and thus improve the efficiency of the European balancing system [20]. Like the INP, a corrective power is introduced to calculate the Area Control Error (ACE) due to the CBRR. The corrective power is calculated by the optimization module of the CBRR and is determined from the actual responses of the participating control units, including the activated regulating reserves [21].

The main difference between the INP and the CBRR lies in the conditions to compensate for the imbalances between participating CAs. The INP is used to avoid the simultaneous activation of regulating reserves with opposite signs in participating CAs, i.e., the compensation is possible between CAs with different signs of demand power. In contrast, the CBRR allows CAs with the same sign of demand power to activate the demand for balancing energy in participating CAs. Both the INP and the CBRR connect all the CAs to a common portal of virtual tie-lines at the ENTSO-E level in continental Europe. The INP and CBRR intend to complement each other, since only the INP or CBRR can perform the compensation at once.

A comprehensive literature review of the used LFC and AGC models for the diverse configurations of power systems are investigated and classified for conventional, modern and future smart power systems. Furthermore, the proposed control strategies for LFC and AGC are studied and categorized into different control groups [22]. An agent-based analysis of the impact of different cross-border balancing arrangements, i.e., separate markets, ACE netting, and balancing energy trade on the performance of the balancing market in northern Europe, is outlined in [23]. Since one of the objectives of the CBRR is to integrate the markets, possible distortions resulting from the insufficient harmonization of national arrangements must be identified, and minimum requirements and long-term recommendations for the implementation of cross-border balancing in Europe must be derived [24]. As such, the possibilities of TSO cooperation for regulating reserve dispatch and procurement must be analyzed in addition to a theoretical analysis of the cross-border reserve cooperation, with a focus on European network codes [25]. An optimization-based method for the cross-border balancing energy exchange and the results from the application of the proposed method to the Swiss transmission grid are shown in [26]. A more cost-effective Europe-wide cross-border activation of the replacement reserve with a novel methodology is suggested for the conversion of balancing energy offers submitted during the integrated scheduling process of the European central-dispatch systems into replacement reserve standards [27]. To increase the financial effects of the CBRR, the dynamic dimensioning of regulating reserves with the CBRR should also be considered [28].

B. CONTRIBUTION AND PAPER STRUCTURE

The compensation of imbalances through the CBRR should positively impact on frequency quality and the provision of LFC. However, this issue needs to be addressed as frequency quality is declining [11]. The impact of the INP on power-system dynamics is shown in [29], which incorporates a frequency term and inherently affects the frequency response of the participating CAs. Since the same control-demand approach is used for the CBRR, the correction power includes load variation and a frequency term. Consequently, the impact of the CBRR is inherent to the frequency response of the participating CAs. To the best of our knowledge, no previous studies have investigated the impact of the CBRR on the power-system dynamics and the provision of LFC. Furthermore, only a limited number of studies have been conducted that consider the cross-border energy trade. The main contributions of this paper are as follows.

- A modified CBRR is proposed that does not affect the eigendynamics of participating CAs.
- The impact of the classic CBRR on the eigendynamics of participating CAs is outlined.
- An eigenvalue analysis of a two-CA system is additionally performed, showing the impact of the tie-line parameter, the inertia time constant, the droop characteristic, and the frequency-bias coefficient.
- The impact of the CBRR on the power-system dynamics and the provision of LFC is thoroughly examined through dynamic simulations with a random load variation.

This paper is organized as follows. Section II describes the basic principle of LFC and the CBRR. Additionally, the classic CBRR optimization is explained, and a modified CBRR is proposed. The impact of the classic and modified CBRR on the dynamics of the power system and the provision of LFC is shown with an eigenvalue analysis of a two-CA system, given in Section III. The impact of the activation factor on the eigenvalues of the system matrix is also evaluated numerically. In Section IV, a three-CA test model with the classic and modified CBRR is described, which was used for dynamic simulations with a random load variation. The results are presented in Section V. First, indicators for the evaluation of the LFC provision are outlined. The results for the standard deviation of the frequency deviation, the standard deviation of the ACE, the mean value of the Rate of Change of Frequency (RoCoF), the unintended exchange of energy and the demand power are presented. Finally, Section VI summarizes the important conclusions and outlines future work.

II. LFC AND CBRR

A. LFC

The frequency of a power system depends on the balance of active power. A change in active-power demand at one point of a power system is reflected in a frequency deviation throughout the entire system. Therefore, the frequency is controlled at a scheduled value. In a large-scale power system consisting of several CAs connected with transmission lines, in addition to the frequency control, the generation within each CA must be controlled to maintain the scheduled power interchanges. Maintaining the frequency and power interchanges with CAs at the scheduled values are the two main objectives of a power system's LFC [12]–[14]. These objectives are achieved by reducing the ACE, which is used as the input signal to the LFC. The power imbalance between generation and consumption is, for the i-th CA, defined as

$$ACE_i' = B_i \Delta f_i + \Delta P_i, \tag{1}$$

where

$$\Delta f_i = (f_{ai} - f_{si}) \tag{2}$$

and

$$\Delta P_i = (P_{ai} - P_{si}) \tag{3}$$

are the frequency deviation and interchange power variation, respectively. Here, f_{ai} and P_{ai} denote the actual, i.e., measured, values, while f_{si} and P_{si} denote the scheduled values. Furthermore, B_i is the frequency-bias coefficient that reflects the size of the CA. The value of B_i is determined on an annual basis by all the TSOs in a synchronous area, taking into account the sum of the primary control reserve in relation to the maximum steady-state frequency deviation,

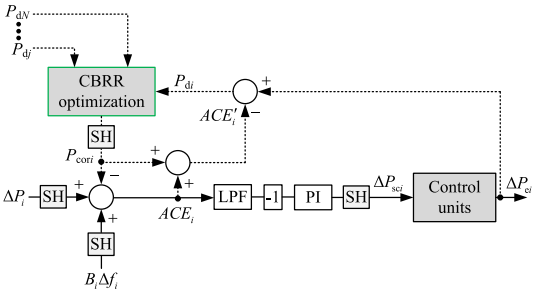

FIGURE 1. Block diagram of the LFC framework of the *i*-th CA (solid line) with the classic CBRR optimization module (solid and dotted line), suggested by ENTSO-E [9].

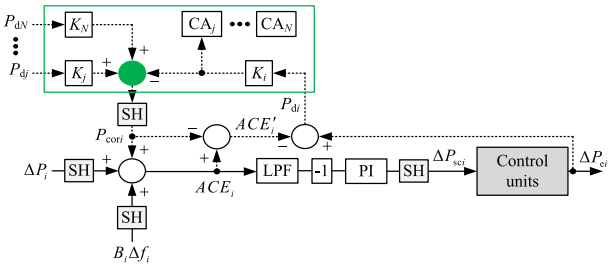

FIGURE 2. Block diagram of the LFC framework of the *i*-th CA (solid line) with the classic CBRR (solid and dotted line).

the auto-control of the generation, and the self-regulation of the load [15]. Furthermore, a CA is characterized as ''short'' if $ACE_i' < 0$, which means that the consumption is higher than the generation. In contrast, a CA is characterized as ''long'' if $ACE_i' > 0$, which means that the generation is higher than the consumption. Note that the terms ''short'' and ''long'' will be used subsequently.

The basic LFC framework of the *i*-th CA is shown in Fig. 1 with a solid line. Here, LPF denotes Low-Pass Filter, which has a maximum cut-off frequency of 0.5 Hz, while SH denotes Sample and Hold, with typical values of a sampling time T_s between 1 to 5 seconds [14]. Furthermore, PI is a Proportional-Integral controller, where a negative control-feedback is included as -1 gain. The output of the LFC is the scheduled control power ΔP_{sci}, which is distributed to the participating control units, which change the actual (electrical) control power ΔP_{ei} accordingly. If the losses are neglected, then ΔP_{ei} is, for the *i*-th CA, defined as

$$\Delta P_{ei} = \Delta P_{Li} + \Delta P_i, \tag{4}$$

where ΔP_{Li} denotes the load-power variation.

The provision of LFC is an expense for the TSO that depends on the size of the actually activated reserve power and the LFC reserve. Note that the term activated reserve power is also known as balancing energy, while the term regulating reserve is typically used instead of LFC reserve.

B. CBRR

CBRR was developed to reduce the expenses associated with the high costs of balancing energy. The block diagram for the classic CBRR, suggested by ENTSO-E [9], is the same as the block diagram for INP. Therefore, the same control-demand approach was suggested. The only difference is that the INP optimization module is substituted with the CBRR optimization module, as shown in Fig. 1. Because of limited literature on CBRR optimization, a more straightforward block diagram is presented for an easier interpretation. This is shown in Fig. 2. Generally, all N CAs can be connected through the virtual tie-lines, i.e., they can all activate the CBRR. Instead of the CBRR optimization module, the activation factors K_i, $K_j, \ldots, K_N$ are added to the block-diagram structure shown in the green rectangle. Note that the factor K_j characterizes the size of the CBRR activation of the *j*-th CA in the *i*-th CA, where $K_j = 0$ means that the possible CBRR activation is equal to 0%, whereas $K_j = 1$ means that the possible CBRR activation is equal to 100%. In addition, the values of $K_i, K_j, \ldots, K_N$ can be different. The participating CAs are connected to the ''green'' summator, thus forming virtual tie-lines, as shown in Fig. 2. Note, a virtual tie-line represents a telemetered reading or value that is updated in real-time and used as a tie-line flow in (1), but for which no physical tie or energy metering actually exists [15]. The input variables to the ''green'' summator are the demand powers of the participating CAs, i.e., $P_{di}, P_{dj}, \ldots, P_{dN}$. The demand power of the *i*-th CA determines the maximum activation power for the *i*-th CA between the participating CAs and is defined as

$$P_{di} = \Delta P_{ei} - ACE_i' \tag{5}$$

according to [9], [12].

By introducing (1) and (4) in (5) the following relation is obtained

$$P_{di} = \Delta P_{Li} - B_i \Delta f_i. \tag{6}$$

The power imbalance between generation and consumption in addition to $K_i P_{di}$ from *i*-th CA, $K_j P_{dj}$ from *j*-th CA, $\ldots, K_N P_{dN}$ from N-th CA is, for the *i*-th CA, defined as

$$ACE_i = B_i \Delta f_i + \Delta P_i - K_i P_{di} + (K_j P_{dj} +, \ldots, +K_N P_{dN}). \tag{7}$$

The output variables of the ''green'' summator are the correction powers of the participating CAs, i.e., P_{cori}, $P_{corj}, \ldots, P_{corN}$, calculated with a delay of T_s due to the SH. The correction power of the *i*-th CA determines the maximum activation power for the *i*-th CA between the participating CAs with the same sign of ACE_i', and is included as

$$ACE_i = (B_i \Delta f_i + \Delta P_i) + P_{cori}, \tag{8}$$

where the terms in brackets denote ACE_i'. Note that ACE_i' does not include a correction term due to the CBRR.

Furthermore, only CAs with the same sign of demand power, i.e., $\text{sign}(P_{di}) = \text{sign}(P_{dj})$, can activate the demand for balancing energy. If any of the participating CAs is ''long'' and the other is ''short'' then INP is used instead of the CBRR and vice versa [30]. Consequently, all the participating CAs must be either ''short'' or ''long'', depending on whether

a positive or negative CBRR is activated. In this way the balancing energy in those CAs that activate the balancing energy in the participating CAs can be reduced, while at the same time the regulating reserve is released. The $P_{\mathrm{cor}i}$, $P_{\mathrm{cor}j}, \ldots, P_{\mathrm{cor}N}$ is calculated by the CBRR optimization module, taking into account various target functions, which is explained in Section II-C.

When considering N CAs, then $P_{\mathrm{cor}i}$ is, for the i-th CA, expressed as

$$P_{\mathrm{cor}i} = -P_{\mathrm{d}i}K_i + P_{\mathrm{d}j}K_j + , \ldots, + P_{\mathrm{d}N}K_N. \tag{9}$$

By considering (6), then the $P_{\mathrm{cor}i}$ between N CAs is, for the i-th CA, expressed as

$$P_{\mathrm{cor}i} = -(\Delta P_{\mathrm{L}i} - B_i\Delta f_i)K_i + (\Delta P_{\mathrm{L}j} - B_j\Delta f_j)K_j + , \ldots, + (\Delta P_{\mathrm{L}N} - B_N\Delta f_N)K_N. \tag{10}$$

Thus, the correction power of the i-th CA compensates the load variation, which is mixed by the frequency deviation of the participating CAs. From a system point of view, this corresponds to an additional frequency-based feedback and cross-couplings with other participating CAs that inherently changes the eigendynamics of the i-th CA.

C. OPTIMIZATION OF THE CBRR

The CBRR optimization module shown in Fig. 1 can be described with the activation factors $K_i, K_j, \ldots, K_N$, which characterize the size of the $P_{\mathrm{d}i}, P_{\mathrm{d}j}, \ldots, P_{\mathrm{d}N}$ activation in the participating CAs, as shown in Fig. 2 and described in Section II-B. The aim of this chapter is merely to present the target functions used by the ENTSO-E optimization module. According to ENTSO-E [9] the common objective function of the CBRR optimization consists of four target functions. The first and most important target function is the largest-possible activation of the balancing energy. Furthermore, the limit of $P_{\mathrm{d}i}$ and the limit of the Available Transmission Capacity (ATC) between the participating CAs, which can be different for each direction of the activation, must be taken into account. The goal is to control the ACE_i' to zero; therefore, the amount of $P_{\mathrm{cor}i}$ to be activated should cover $P_{\mathrm{d}i}$. In addition, the amount of activated $P_{\mathrm{d}i}$ in the i-th CA should be minimized and should be activated in the j-th CA. The second is the target function of fairness, which splits the $P_{\mathrm{d}i}$ between the participating CAs when multiple CAs are connected by a common point. In the case of parallel tie-lines, the third target function is required for the advantageous use of the tie-lines with the highest ATC. In addition, the fourth target function is also possible for an economic optimization that minimizes the costs of the participating CAs. Only the economically most efficient bids for $P_{\mathrm{d}i}$ activation should be chosen. Note that CBRR optimization is not used and discussed in this paper. The aim of this paper is to show the impact of the CBRR on the power-system dynamics and the provision of LFC, regardless of whether the activation factors $K_i, K_j, \ldots, K_N$ are chosen optimally or not.

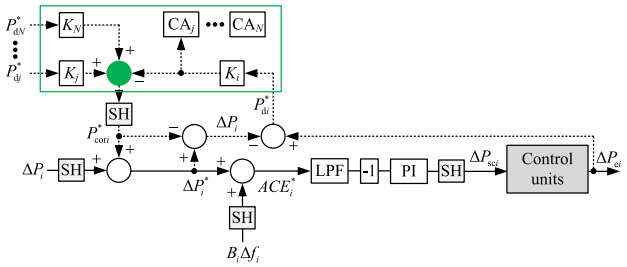

FIGURE 3. Block diagram of the LFC framework of the i-th CA (solid line) with modified implementation of the CBRR (solid and dotted line).

D. MODIFIED CBRR

The demand power $P_{\mathrm{d}i}$ of a CBRR includes a frequency term, as expressed by (6), which is reflected in the correction power $P_{\mathrm{cor}i}$, as is expressed by (10). Furthermore, the activation between the i-th and j-th CA is only possible if $\mathrm{sign}(P_{\mathrm{d}i}) = \mathrm{sign}(P_{\mathrm{d}j})$. This condition might not be fulfilled for the frequency term in (6), i.e., $\mathrm{sign}(\Delta P_{\mathrm{L}i}) = \mathrm{sign}(\Delta P_{\mathrm{L}j})$, although cases of $\mathrm{sign}(\Delta f_i) \neq \mathrm{sign}(\Delta f_j)$, exist in the transient state. Consequently, the correction of the frequency term in one CA would be incorrect. Hence, the motivation for changing the CBRR implementation was suggested as one of the contributions of this paper, as shown in Fig. 3 with a solid and a dotted line. Generally, all N CAs can activate the modified CBRR. The CBRR shown in Fig. 2 is further referred to as the classic CBRR to distinguish it from the proposed, i.e., the modified CBRR. However, only the implementation of the CBRR in the LFC framework is changed, whereas the CBRR optimization module, suggested by ENTSO-E [9], is not. Thus, the modified demand power is given as

$$P^*_{\mathrm{d}i} = \Delta P_{\mathrm{e}i} - \Delta P_i \tag{11}$$

and when introducing (4) in (11) it results in

$$P^*_{\mathrm{d}i} = \Delta P_{\mathrm{L}i}. \tag{12}$$

The output variables of the green summator are modified correction powers of the participating CAs, i.e., $P^*_{\mathrm{cor}i}$, $P^*_{\mathrm{cor}j}, \ldots, P^*_{\mathrm{cor}N}$, calculated with a delay of T_{s} due to the SH, which is included for the i-th CA as

$$ACE^*_i = (B_i\Delta f_i + \Delta P_i) + P^*_{\mathrm{cor}i}. \tag{13}$$

Furthermore, when considering N CAs, similar to in Section II-B, then the modified $P^*_{\mathrm{cor}i}$ is, for the i-th CA, expressed as

$$P^*_{\mathrm{cor}i} = -\Delta P_{\mathrm{L}i}K_i + \Delta P_{\mathrm{L}j}K_j + , \ldots, + \Delta P_{\mathrm{L}N}K_N. \tag{14}$$

In contrast to the classic CBRR, only the load variation is compensated in this way. Consequently, the eigendynamics of the i-th CA is not affected.

A thorough analysis of the impact of the modified CBRR is given in the following and the advantages over the classic CBRR are shown undoubtedly.

III. EIGENVALUE ANALYSIS OF A TWO-CA SYSTEM WITH THE CLASSIC AND MODIFIED CBRR

A linearized 4th-order system with constant parameters is used to describe the i-th CA, as proposed in [12], [14]. The generator-load dynamics are represented by the inertia time constant H_i and the damping coefficient D_i. A governor-and-turbine system is described as a steam non-reheat turbine with the time constants T_{Gi} and T_{CHi}, respectively. A primary frequency loop with a constant droop characteristic R_i is considered. Furthermore, the LFC is modeled by a PI controller with a gain K_{ri} and a time constant T_{ri}. In addition, the classic and modified CBRR are also included according to Fig. 2 and Fig. 3, where the activation factor K_i characterizes the size of the activation of P_{di} in the j-th CA, whereas K_j characterizes the size of the activation of P_{dj} in the i-th CA, as described in Section II-B. The tie-line between CA_i–CA_j is described by a synchronizing coefficient T_{ij} [31]. Note that the LPF and the time delays due to the SH are not considered.

A. STATE-SPACE MODEL

Two CAs connected by a tie-line represent a 9th-order system, which is given in the state-space matrix representation as

$$\dot{\mathbf{x}} = \mathbf{A}\mathbf{x} + \mathbf{B}\mathbf{u}. \tag{16}$$

The vectors of the state-space and input variables are given, respectively, as

$$\mathbf{x}^{\mathrm{T}} = [\Delta f_1, \Delta P_{\mathrm{m1}}, \Delta P_{\mathrm{g1}}, \int ACE_1\, dt, \Delta f_2, \Delta P_{\mathrm{m2}}, \Delta P_{\mathrm{g2}}, \int ACE_2 dt, \Delta P_{12}] \tag{17}$$

and

$$\mathbf{u}^{\mathrm{T}} = [\Delta P_{\mathrm{L1}}, \Delta P_{\mathrm{L2}}]. \tag{18}$$

Here, ΔP_{m1} and ΔP_{m2} are the turbine outputs, whereas ΔP_{g1} and ΔP_{g2} are the governor outputs. For the two participating, i.e., CA_1 and CA_2, the only possible corrections are given as

$$P_{\mathrm{cor1}} = -P_{\mathrm{d1}}K_1 + P_{\mathrm{d2}}K_2 \tag{19}$$

and

$$P_{\mathrm{cor2}} = -P_{\mathrm{d2}}K_2 + P_{\mathrm{d1}}K_1 \tag{20}$$

due to the classic or modified CBRR. Furthermore, the system and the input matrices $\mathbf{A}$ and $\mathbf{B}$ depend on the type of the CBRR being used. When considering the classic CBRR given in Section II-B, then the matrices $\mathbf{A}$ and $\mathbf{B}$ are given by (15), as shown at the bottom of the page. When considering the modified CBRR given in Section II-D, then the matrix $\mathbf{A}$ corresponds to a system without a CBRR, i.e., $K_1 = 0$ and $K_2 = 0$, which is one of the contributions of this paper. However, for a system with the classic and modified CBRR, both have the same input matrix $\mathbf{B}$. The impact of the activation factors K_1 and K_2 on the matrices $\mathbf{A}$ and $\mathbf{B}$ is summarized in Table 1. Considering (10) and (14) means that Table 1 applies to a system with N CAs.

TABLE 1. Impact of the activation factors K_1 and K_2 on the matrices A and B.

matrix	without CBRR	classic CBRR	modified CBRR
A	NO	YES	NO
B	NO	YES	YES

B. NUMERICAL EVALUATION OF THE IMPACT OF THE ACTIVATION FACTORS K_1 AND K_2 ON THE EIGENVALUES OF A

A numerical evaluation of the impact of the activation factors K_1 and K_2 on the eigenvalues of $\mathbf{A}$ is performed, since exact analytical expressions for the eigenvalues are complicated. Note that the determination of optimal activation factors K_1 and K_2 are not studied in this paper. Two identical CAs were assumed, with typical parameters and control settings [12], [14] that are summarized in Table 4. Note, the only differences between the CAs were the PI controller time constants, which were $T_{\mathrm{r1}} = 60$ s and $T_{\mathrm{r2}} = 30$ s. Moreover, for the two CAs, only two corrections are meaningful. When considering $K_2 = 0$ and $0 \geq K_1 \geq 1$, then $P_{\mathrm{cor1}} = -P_{\mathrm{d1}}K_1$ and $P_{\mathrm{cor2}} = P_{\mathrm{d1}}K_1$. When considering $K_1 = 0$ and $0 \geq K_2 \geq 1$, then $P_{\mathrm{cor1}} = P_{\mathrm{d2}}K_2$ and $P_{\mathrm{cor2}} = -P_{\mathrm{d2}}K_2$. Only the classic

$$\mathbf{A} = \begin{bmatrix}
-\frac{D_1}{2H_1} & \frac{1}{2H_1} & 0 & 0 & 0 & 0 & 0 & 0 & -\frac{1}{2H_1} \\
0 & -\frac{1}{T_{\mathrm{CH1}}} & \frac{1}{T_{\mathrm{CH1}}} & 0 & 0 & 0 & 0 & 0 & 0 \\
-\frac{1+R_1K_{\mathrm{r1}}B_1(1+K_1)}{R_1T_{\mathrm{G1}}} & 0 & -\frac{1}{T_{\mathrm{G1}}} & -\frac{K_{\mathrm{r1}}}{T_{\mathrm{G1}}T_{\mathrm{r1}}} & \frac{K_{\mathrm{r1}}B_2K_2}{T_{\mathrm{G1}}} & 0 & 0 & 0 & -\frac{K_{\mathrm{r1}}}{T_{\mathrm{G1}}} \\
B_1(1+K_1) & 0 & 0 & 0 & -B_2K_2 & 0 & 0 & 0 & 1 \\
0 & 0 & 0 & 0 & -\frac{D_2}{2H_2} & \frac{1}{2H_2} & 0 & 0 & \frac{1}{2H_2} \\
0 & 0 & 0 & 0 & 0 & -\frac{1}{T_{\mathrm{CH2}}} & \frac{1}{T_{\mathrm{CH2}}} & 0 & 0 \\
\frac{K_{\mathrm{r2}}B_1K_1}{T_{\mathrm{G2}}} & 0 & 0 & 0 & -\frac{1+R_2K_{\mathrm{r2}}B_2(1+K_2)}{R_2T_{\mathrm{G2}}} & 0 & -\frac{1}{T_{\mathrm{G2}}} & -\frac{K_{\mathrm{r2}}}{T_{\mathrm{G2}}T_{\mathrm{r2}}} & \frac{K_{\mathrm{r2}}}{T_{\mathrm{G2}}} \\
-B_1K_1 & 0 & 0 & 0 & B_2(1+K_2) & 0 & 0 & 0 & -1 \\
2\pi T_{12} & 0 & 0 & 0 & -2\pi T_{12} & 0 & 0 & 0 & 0
\end{bmatrix}, \mathbf{B} = \begin{bmatrix}
-\frac{1}{2H_1} & 0 \\
0 & 0 \\
\frac{K_{\mathrm{r1}}K_1}{T_{\mathrm{G1}}} & -\frac{K_{\mathrm{r1}}K_2}{T_{\mathrm{G1}}} \\
-K_1 & K_2 \\
0 & -\frac{1}{2H_2} \\
0 & 0 \\
-\frac{K_{\mathrm{r2}}K_1}{T_{\mathrm{G2}}} & \frac{K_{\mathrm{r2}}K_2}{T_{\mathrm{G2}}} \\
K_1 & -K_2 \\
0 & 0
\end{bmatrix} \tag{15}$$

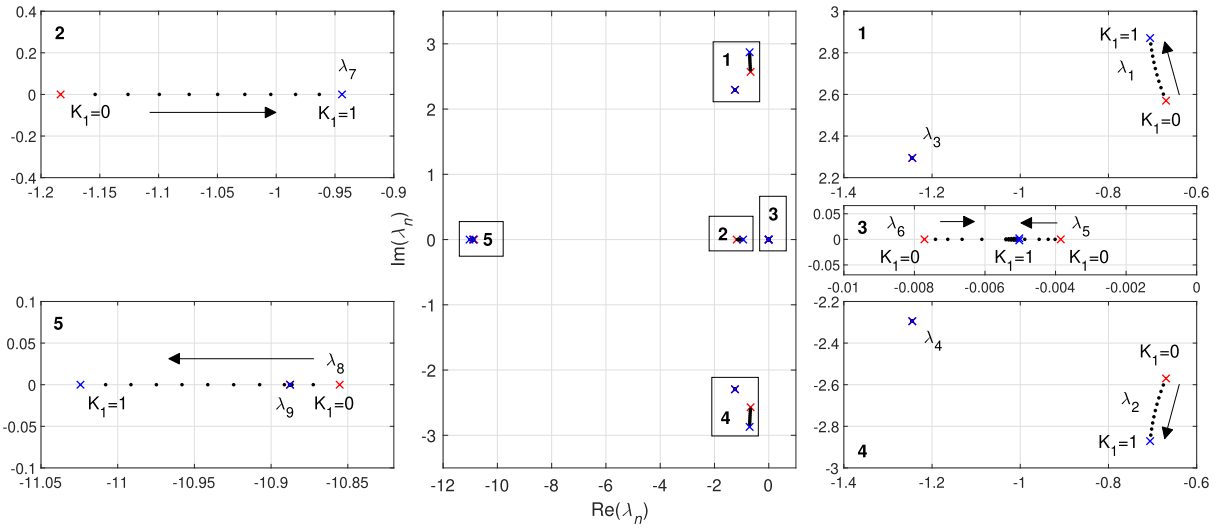

FIGURE 4. Impact of the activation factor K_1, while $K_2 = 0$ on the eigenvalues of **A** for the system with the classic CBRR.

TABLE 2. Coefficients of a characteristic polynomial.

a_n	K_1 free parameter, $K_2 = 0$	a_n	K_2 free parameter, $K_1 = 0$
a_0	0.2	a_0	0.2
a_1	-9.8K_1+78	a_1	10K_2+80
a_2	28K_1+6800	a_2	50K_2+7000
a_3	1280K_1+10800	a_3	1300K_2+10500
a_4	580K_1+7400	a_4	600K_2+7500
a_5	240K_1+3600	a_5	230K_2+3700
a_6	17.2K_1+1120	a_6	17K_2+1100
a_7	255	a_7	255
a_8	27	a_8	27
a_9	1	a_9	1

CBRR is considered, since it affects the matrix **A** according to Table 1. The obtained characteristic polynomial is given as

$$\sum_{n=0}^{9} a_n \lambda^n, \tag{21}$$

where λ is an eigenvalue of **A**, while the coefficients a_n are given in Table 2 for both the discussed corrections.

The impact of the activation factor K_1, while $K_2 = 0$ on the eigenvalues of **A** for the classic CBRR is shown in Fig. 4. The most critical are the complex conjugate eigenvalues λ_1 and λ_2. Increasing the activation factor K_1, while $K_2 = 0$ results in a decrease of the damping ζ of λ_1 and λ_2, as given in Table 3, and has a negative impact on the system eigendynamics. Similar conclusion can be made also when increasing the activation factor K_1, while $K_2 = 0.5$ or $K_2 = 1$. However, such cases, where both of the two participating CAs activate CBRR simultaneously, i.e, CA_1 in CA_2 and vice versa, are not meaningful.

According to [32], [33], the tie-line parameter T_{ij}, the inertia time constant H_i and the droop characteristic R_i have a major impact on frequency stability. Different values of T_{ij}, H_i and R_i were used to show the impact of the activation factor K_1, while $K_2 = 0$ on the damping of the dominant

TABLE 3. Impact of the activation factors K_1 and K_2 on the damping of the dominant complex conjugate eigenvalues λ_1 and λ_2 of **A**.

K_1	K_2	ζ	K_1	K_2	ζ	K_1	K_2	ζ
0	0	0.2519	0	0.5	0.2441	0	1	0.2352
0.1	0	0.2512	0.1	0.5	0.2426	0.1	1	0.2333
0.2	0	0.2501	0.2	0.5	0.2410	0.2	1	0.2313
0.3	0	0.2488	0.3	0.5	0.2391	0.3	1	0.2292
0.4	0	0.2472	0.4	0.5	0.2371	0.4	1	0.2269
0.5	0	0.2454	0.5	0.5	0.2350	0.5	1	0.2246
0.6	0	0.2434	0.6	0.5	0.2328	0.6	1	0.2223
0.7	0	0.2412	0.7	0.5	0.2305	0.7	1	0.2199
0.8	0	0.2390	0.8	0.5	0.2281	0.8	1	0.2174
0.9	0	0.2366	0.9	0.5	0.2257	0.9	1	0.2150
1	0	0.2342	1	0.5	0.2232	1	1	0.2125

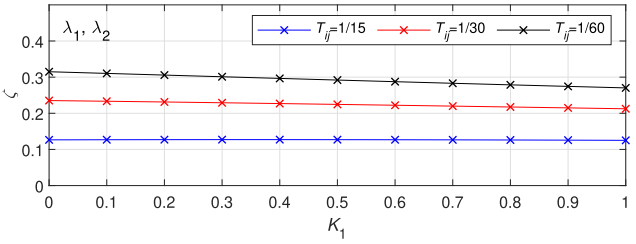

FIGURE 5. Impact of the activation factor K_1, while $K_2 = 0$ on the damping of the complex conjugate eigenvalues λ_1 and λ_2 of **A** for different values of T_{ij}.

eigenvalues λ_1 and λ_2 of **A**. Furthermore, the frequency-bias coefficient B_i was also varied. In Fig. 5 it is clear that an increase of T_{ij} results in a decrease of ζ, in addition to the decrease of ζ with the increase of K_1 for the eigenvalues λ_1 and λ_2. In Fig. 6 it is clear that an increase of H_i results in an increase of ζ, in addition to the decrease of ζ with the increase of K_1 for the eigenvalues λ_1 and λ_2. In Fig. 7 two cases were considered. First, a case was assumed, where B_i was varied, while $R_i = 1/(B_i - D_i)$ [12], which is shown with the dashed lines. Second, the value of B_i was constant and set as 0.3433 pu/Hz, while R_i was varied, which is shown with

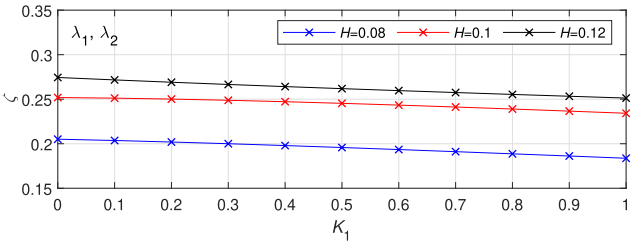

FIGURE 6. Impact of the activation factor K_1, while $K_2 = 0$ on the damping of the complex conjugate eigenvalues λ_1 and λ_2 of **A** for different values of H_i.

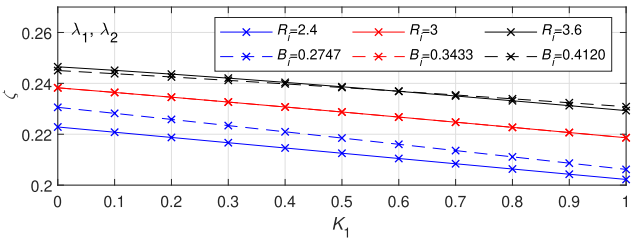

FIGURE 7. Impact of the activation factor K_1, while $K_2 = 0$ on the damping of the complex conjugate eigenvalues λ_1 and λ_2 of **A** for different values of R_i (solid line) and B_i (dashed line).

the solid lines. It is clear that an increase of R_i as well as B_i results in an increase of ζ, in addition to the decrease of ζ with the increase of K_1 for the eigenvalues λ_1 and λ_2. Note that the results obtained for considering the activation factor K_2 as a free parameter, while $K_1 = 0$ are similar.

IV. DYNAMIC SIMULATIONS

A three-CA test system was considered in which CA_1–CA_2 and CA_2–CA_3 were connected with physical tie-lines, while CA_1–CA_3 were not connected by a tie-line. In addition, all three CAs were connected by virtual tie-lines due to the CBRR. A Matlab/SIMULINK model was developed in which dynamic simulations were performed with a step size of 50 ms.

A. DYNAMIC MODEL

1) STRUCTURE

To test the classic and modified CBRR, an individual CA was described with a linearized, low-order, time-invariant model [14], [34], as shown in Fig. 8. Note that the classic and modified CBRR are not shown so as to make the figure more transparent. The model assumes that the voltage control (reactive power) does not impact on the frequency control (active power). Furthermore, a group of multiple generators was replaced by one equivalent, neglecting the fast dynamic of voltage and angle, which reduced the complexity of the modeling. Therefore, the generator-load dynamics are described by the inertia time constant H_i and the damping coefficient D_i that accounts for the frequency dependence of the CA load. In addition, three different types of governor-turbine systems were considered, i.e., a steam non-reheat unit,

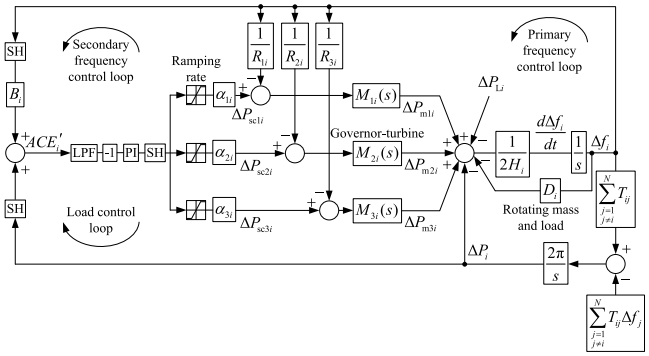

FIGURE 8. Block diagram of the i-th CA.

a steam reheat unit and a hydraulic unit, which are presented with the following transfer functions

$$M_{1i} = \frac{1}{sT_{\mathrm{CH}i}+1}\frac{1}{sT_{\mathrm{G}i}+1}, \tag{22}$$

$$M_{2i} = \frac{sF_{\mathrm{HP}i}T_{\mathrm{RH}i}+1}{(sT_{\mathrm{CH}i}+1)(sT_{\mathrm{RH}i}+1)}\frac{1}{sT_{\mathrm{G}i}+1}, \tag{23}$$

$$M_{3i} = \frac{sT_{\mathrm{R}i}+1}{(R_{\mathrm{T}i}/R_{\mathrm{P}i})sT_{\mathrm{R}i}+1}\frac{-sT_{\mathrm{W}i}+1}{s0.5T_{\mathrm{W}i}+1}\frac{1}{sT_{\mathrm{G}i}+1}, \tag{24}$$

respectively [12]. Here, $T_{\mathrm{CH}i}$ is the time constant of the main inlet volume and steam chest, $F_{\mathrm{HP}i}$ is a fraction of the total turbine power generated by the high-pressure turbine section, $T_{\mathrm{RH}i}$ is the time constant of the re-heater, $T_{\mathrm{R}i}$ is the reset time, $R_{\mathrm{T}i}$ is the temporary droop, $R_{\mathrm{P}i}$ is the permanent droop, $T_{\mathrm{W}i}$ is the water start time and $T_{\mathrm{G}i}$ denotes the governor time constant. The tie-line connection to the neigboring CAs is described by T_{ij}, which is defined by the line reactance, magnitude and angle difference of the line terminal bus voltage [31]. The ramping rate and participation factors $\alpha_{\mathrm{k}i}$ of the control units were considered in addition to a constant droop characteristic $R_{\mathrm{k}i}$. Furthermore, a PI controller and a 1st-order LPF were modeled as

$$G_{\mathrm{r}i} = \frac{K_{\mathrm{r}i}(sT_{\mathrm{r}i}+1)}{sT_{\mathrm{r}i}}, \tag{25}$$

$$G_{\mathrm{LPF}i} = \frac{1}{sT_{\mathrm{LPF}i}+1}, \tag{26}$$

where the gain and time constant of the PI controller are denoted as $K_{\mathrm{r}i}$ and $T_{\mathrm{r}i}$. The LPF time constant is denoted as $T_{\mathrm{LPF}i}$. Moreover, three different structures were modeled, i.e., with the modified CBRR, with the classic CBRR and without the CBRR.

2) PARAMETERS

The parameters of the model used for the dynamic simulations are specified in Table 4. They are defined according to [12], [14] for the discussed three-CA dynamic model. The model parameters were set to be the same for all three CAs. The only differences were the PI controller time constants $T_{\mathrm{r}i}$. The frequency-bias coefficient was determined as a constant, defined as

$$B_i = 1/R_{1i} + 1/R_{2i} + 1/R_{3i} + D_i \tag{27}$$

TABLE 4. Model parameters used for dynamic simulations.

parameter	value	parameter	value	parameter	value
H_i	0.1 pu s	α_{ki}	1/3	$T_{\mathrm{LPF}i}$	0.3 s
D_i	0.01 pu/Hz	K_{ri}	0.3	T_{r1}	60 s
T_{ij}	1/30 pu/Hz	R_{ki}	3 Hz/pu	$T_{\mathrm{r2}} = T_{\mathrm{r3}}$	30 s
hydraulic	value	non-rehat	value	reheat	value
$T_{\mathrm{G}i}$	0.2 s	$T_{\mathrm{G}i}$	0.1 s	$T_{\mathrm{G}i}$	0.2 s
$T_{\mathrm{R}i}$	5 s	$T_{\mathrm{CH}i}$	0.3 s	$T_{\mathrm{RH}i}$	7 s
$T_{\mathrm{W}i}$	1 s	–	–	$T_{\mathrm{CH}i}$	0.3 s
$R_{\mathrm{T}i}/R_{\mathrm{P}i}$	7.6	–	–	$F_{\mathrm{HP}i}$	0.3
ramp rate	±100	ramp rate	±20	ramp rate	±10

and the ramp rate is given in puMW/min. In addition, a cycle of the AGC and the classic or modified CBRR with $T_{\mathrm{s}} = 2$ s was included.

3) RANDOM LOAD VARIATION

Two components were used to model the load variation [35]. A low-frequency component was obtained as a moving average per hour, whereas the residual component captures variations with a quasi-period of several minutes. Both components were described with a linear stochastic, time-invariant, first-order system

$$\begin{aligned} z(t+1) &= \rho_L z(t) + bw(t) \\ \Delta P_L(t) &= z(t) + \mu_L \end{aligned} \tag{28}$$

where $z(t)$ is a state variable and $w(t) \sim N(0, 1)$ is Gaussian white noise. Furthermore, $b = \sigma_L\sqrt{1-\rho_L^2}$, and the parameters σ_L, μ_L and ρ_L, respectively, denote the standard deviation, mean value and auto-correlation of the random load. All the statistical parameters were estimated based on measurements of an open-loop ACE in an undisclosed CA for a time period of 24 hours. The random load variation was obtained by the superposition of both the discussed components and was changed every 60 s. Fig. 9 shows the resulting normalized loads for three CAs with different magnitudes. Note that the load proportions were kept constant and set as $\Delta P_{\mathrm{L1}}/\Delta P_{\mathrm{L2}} = 2/3$, $\Delta P_{\mathrm{L2}}/\Delta P_{\mathrm{L3}} = 3/4$ and $\Delta P_{\mathrm{L1}}/\Delta P_{\mathrm{L3}} = 1/2$.

B. TEST CASES

The loads of the individual CAs were changed simultaneously, having the same sign, i.e., all three CAs were either short or long. A condition for the CBRR activation at all times of the simulation was ensured in this way. In addition, the limit of the ATC for power interchange between neighboring CAs was not considered, to achieve maximum activation with the classic and modified CBRR. Two test cases of $P_{\mathrm{d}i}$ activation in the neighboring CAs were considered for the dynamic simulations of a three-CA test system, as shown in Table 5. In Case 1 CA_2 activated from 0% to 50% of P_{d2} in CA_1 and CA_3. In Case 2 CA_1 and CA_3 activated from 0% to 100% of P_{d1} and P_{d3} in CA_2. In addition, subcases a–f were considered as, given in Tables 6 and 7.

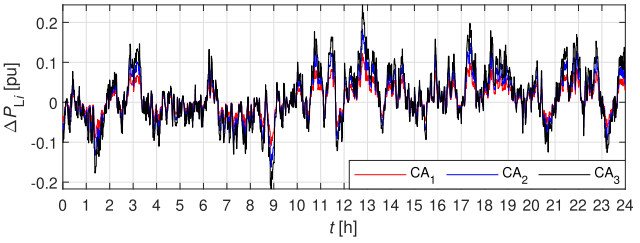

FIGURE 9. Random variations of ΔP_{Li} for a three CA test system.

TABLE 5. Amount of P_{di} activation for a three CA test system.

	CA_1	CA_2	CA_3
Case 1	0 P_{d2}	1 P_{d2}	0 P_{d2}
	0.1 P_{d2}	0.8 P_{d2}	0.1 P_{d2}
	0.2 P_{d2}	0.6 P_{d2}	0.2 P_{d2}
	0.3 P_{d2}	0.4 P_{d2}	0.3 P_{d2}
	0.4 P_{d2}	0.2 P_{d2}	0.4 P_{d2}
	0.5 P_{d2}	0 P_{d2}	0.5 P_{d2}
Case 2	1 P_{d1}	0 P_{d1} and 0 P_{d3}	1 P_{d3}
	0.8 P_{d1}	0.2 P_{d1} and 0.2 P_{d3}	0.8 P_{d3}
	0.6 P_{d1}	0.4 P_{d1} and 0.4 P_{d3}	0.6 P_{d3}
	0.4 P_{d1}	0.6 P_{d1} and 0.6 P_{d3}	0.4 P_{d3}
	0.2 P_{d1}	0.8 P_{d1} and 0.8 P_{d3}	0.2 P_{d3}
	0 P_{d1}	1 P_{d1} and 1 P_{d3}	0 P_{d3}

V. RESULTS

For a test system with three CAs, dynamic simulations were performed to analyze the impact of the classic and modified CBRR on the system's response. Indicators were used to evaluate the LFC provision, i.e., performance indicators, RoCoF, unintended exchange of energy and demand power. The impact was evaluated according to the results obtained.

A. PERFORMANCE INDICATORS

The quality of the frequency is evaluated with the Standard Deviation of Δf_i, denoted as $\sigma_{\Delta f_i}$, which is given in [15], [36]. The term frequency quality can also be used as a measure of the maintenance of the balance between the generation and consumption of electrical energy in the power system [37]. In addition, the provision of the LFC is typically assessed using indicators defined by Control Performance Standards (CPS) [15], [36]. The Standard Deviation of ACE_i, denoted as σ_{ACE_i}, is used as a common indicator that is also comparable to the performance criterion defined by the ENTSO-E [38]. It is also comparable to CPS2 given by the North American Electric Reliability Corporation (NERC) [36]. Note that 15-minute averages, as defined in [15], of the discussed variables have been taken into account.

The results of $\sigma_{\Delta f_i}$ are shown in Fig. 10 left for Case 1 and right for Case 2. In Case 1 the classic CBRR reduced $\sigma_{\Delta f_1}$ and $\sigma_{\Delta f_3}$ in CAs, which activated KP_{d2}, while $\sigma_{\Delta f_2}$ was increased with the increase of K. The modified CBRR additionally reduced $\sigma_{\Delta f_1}$ and $\sigma_{\Delta f_3}$, whereas $\sigma_{\Delta f_2}$ was also reduced in contrast to the classic CBRR. In Case 2 classic CBRR reduced $\sigma_{\Delta f_1}$, increased in $\sigma_{\Delta f_3}$, while $\sigma_{\Delta f_2}$ in CA, which activated KP_{d1} and KP_{d3}, was reduced with the increase of K. The modified CBRR

TABLE 6. Amount of P_{di} activation in Cases 1 a–f for a three CA test system.

	CA_1	CA_2						CA_3					
	a–f	a	b	c	d	e	f	a	b	c	d	e	f
Cases 1 a–f	0 P_{d2}	1 P_{d2}	0.9 P_{d2}	0.8 P_{d2}	0.7 P_{d2}	0.6 P_{d2}	0.5 P_{d2}	0 P_{d2}	0.1 P_{d2}	0.2 P_{d2}	0.3 P_{d2}	0.4 P_{d2}	0.5 P_{d2}
	0.1 P_{d2}	0.9 P_{d2}	0.8 P_{d2}	0.7 P_{d2}	0.6 P_{d2}	0.5 P_{d2}	0.4 P_{d2}	0 P_{d2}	0.1 P_{d2}	0.2 P_{d2}	0.3 P_{d2}	0.4 P_{d2}	0.5 P_{d2}
	0.2 P_{d2}	0.8 P_{d2}	0.7 P_{d2}	0.6 P_{d2}	0.5 P_{d2}	0.4 P_{d2}	0.3 P_{d2}	0 P_{d2}	0.1 P_{d2}	0.2 P_{d2}	0.3 P_{d2}	0.4 P_{d2}	50 P_{d2}
	0.3 P_{d2}	0.7 P_{d2}	0.6 P_{d2}	0.5 P_{d2}	0.4 P_{d2}	0.3 P_{d2}	0.2 P_{d2}	0 P_{d2}	0.1 P_{d2}	0.2 P_{d2}	0.3 P_{d2}	0.4 P_{d2}	0.5 P_{d2}
	0.4 P_{d2}	0.6 P_{d2}	0.5 P_{d2}	0.4 P_{d2}	0.3 P_{d2}	0.2 P_{d2}	0.1 P_{d2}	0 P_{d2}	0.1 P_{d2}	0.2 P_{d2}	0.3 P_{d2}	0.4 P_{d2}	0.5 P_{d2}
	0.5 P_{d2}	0.5 P_{d2}	0.4 P_{d2}	0.3 P_{d2}	0.2 P_{d2}	0.1 P_{d2}	0 P_{d2}	0 P_{d2}	0.1 P_{d2}	0.2 P_{d2}	0.3 P_{d2}	0.4 P_{d2}	0.5 P_{d2}

TABLE 7. Amount of P_{di} activation in Cases 2 a–f for a three CA test system.

	CA_1	CA_2						CA_3					
	a–f	a–f	a	b	c	d	e	f	a	b	c	d	e	f
Cases 2 a–f	1 P_{d1}	0 P_{d1}	0 P_{d3}	0.2 P_{d3}	0.4 P_{d3}	0.6 P_{d3}	0.8 P_{d3}	1 P_{d3}	1 P_{d3}	0.8 P_{d3}	0.6 P_{d3}	0.4 P_{d3}	0.2 P_{d3}	0 P_{d3}
	0.8 P_{d1}	0.2 P_{d1}	0 P_{d3}	0.2 P_{d3}	0.4 P_{d3}	0.6 P_{d3}	0.8 P_{d3}	1 P_{d3}	1 P_{d3}	0.8 P_{d3}	0.6 P_{d3}	0.4 P_{d3}	0.2 P_{d3}	0 P_{d3}
	0.6 P_{d1}	0.4 P_{d1}	0 P_{d3}	0.2 P_{d3}	0.4 P_{d3}	0.6 P_{d3}	0.8 P_{d3}	1 P_{d3}	1 P_{d3}	0.8 P_{d3}	0.6 P_{d3}	0.4 P_{d3}	0.2 P_{d3}	0 P_{d3}
	0.4 P_{d1}	0.6 P_{d1}	0 P_{d3}	0.2 P_{d3}	0.4 P_{d3}	0.6 P_{d3}	0.8 P_{d3}	1 P_{d3}	1 P_{d3}	0.8 P_{d3}	0.6 P_{d3}	0.4 P_{d3}	0.2 P_{d3}	0 P_{d3}
	0.2 P_{d1}	0.8 P_{d1}	0 P_{d3}	0.2 P_{d3}	0.4 P_{d3}	0.6 P_{d3}	0.8 P_{d3}	1 P_{d3}	1 P_{d3}	0.8 P_{d3}	0.6 P_{d3}	0.4 P_{d3}	0.2 P_{d3}	0 P_{d3}
	0 P_{d1}	1 P_{d1}	0 P_{d3}	0.2 P_{d3}	0.4 P_{d3}	0.6 P_{d3}	0.8 P_{d3}	1 P_{d3}	1 P_{d3}	0.8 P_{d3}	0.6 P_{d3}	0.4 P_{d3}	0.2 P_{d3}	0 P_{d3}

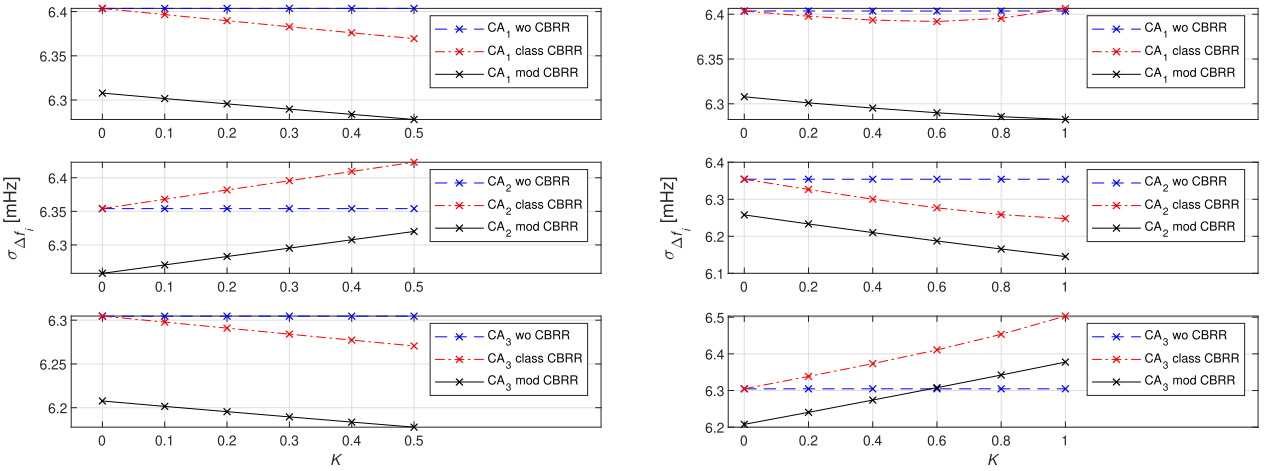

FIGURE 10. Values of $\sigma_{\Delta f_i}$ for Case 1 (left) and Case 2 (right) in relation to K.

additionally reduced $\sigma_{\Delta f_i}$ in all three CAs, in contrast to the classic CBRR.

Fig. 11 shows an average value of $\sigma_{\Delta f_i}$, left for Cases 1 a–f and right for Cases 2 a–f. In all cases the modified CBRR reduced $\sigma_{\Delta f_i}$ in all three CAs in comparison to the classic CBRR.

The results of σ_{ACE_i} are shown in Fig. 12 left for Case 1 and right for Case 2. In Case 1 the classic CBRR increased σ_{ACE_1} and σ_{ACE_3} in CAs, which activated KP_{d2}, while σ_{ACE_2} was reduced with the increase of K. The values of σ_{ACE_1} and σ_{ACE_3} due to the modified CBRR, were also increased in comparison to the system without the CBRR; however, σ_{ACE_i} was reduced in comparison to classic CBRR. Furthermore σ_{ACE_2} was additionally reduced with modified CBRR. In Case 2 classic CBRR reduced σ_{ACE_1} and σ_{ACE_3}, while σ_{ACE_2} in CA, which activated KP_{d1} and KP_{d3}, was increased with the increase of K. The values of σ_{ACE_1} and σ_{ACE_3} due to the modified CBRR were also reduced in comparison to the system without CBRR; however, σ_{ACE_2} was increased. Furthermore, σ_{ACE_i} in all three CAs was additionally reduced with the modified CBRR in comparison to the classic CBRR.

Fig. 13 shows the results of an average value of σ_{ACE_i}, left for Cases 1 a–f and right for Cases 2 a–f. In Cases 1 a–f σ_{ACE_1} and σ_{ACE_3} were reduced in CAs, which activated KP_{d2}, while $\sigma_{\Delta ACE_2}$ was either increased or reduced with the modified CBRR in comparison to the classic CBRR. In Cases 2 a–f σ_{ACE_1} and σ_{ACE_2} were reduced, while σ_{ACE_3} was either increased or reduced with the modified CBRR in comparison to the classic CBRR; however, the differences were negligible.

B. RoCoF

According to [39] this is the time derivative of the power system's frequency, i.e., $\frac{df_i}{dt}$. Traditionally, it has been of little importance for power systems whose generation is based mainly on synchronous generators (SGs), since the inertia

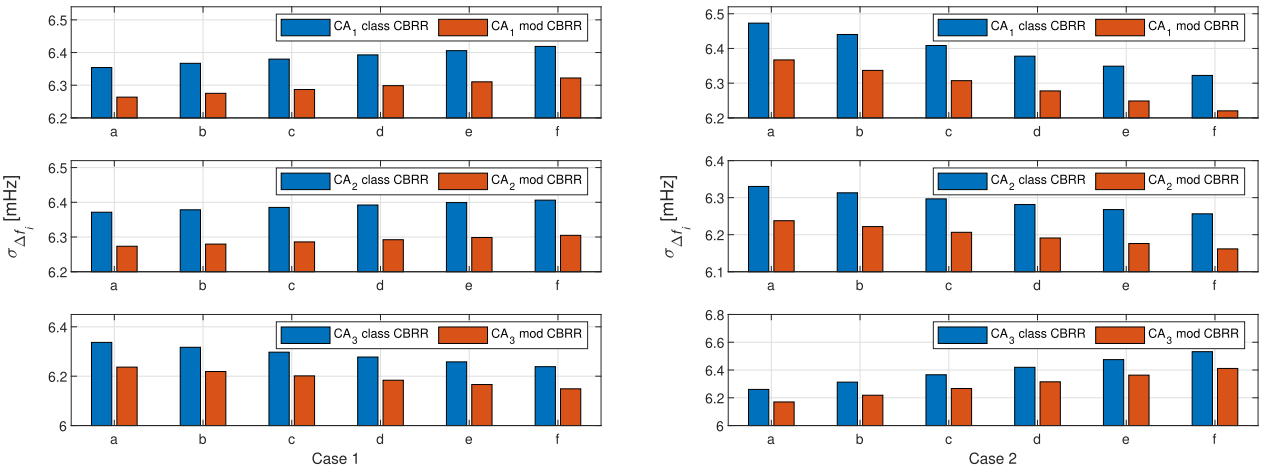

FIGURE 11. Average values of $\sigma_{\Delta f_i}$ for Cases 1 a–f (left) and Cases 2 a–f (right).

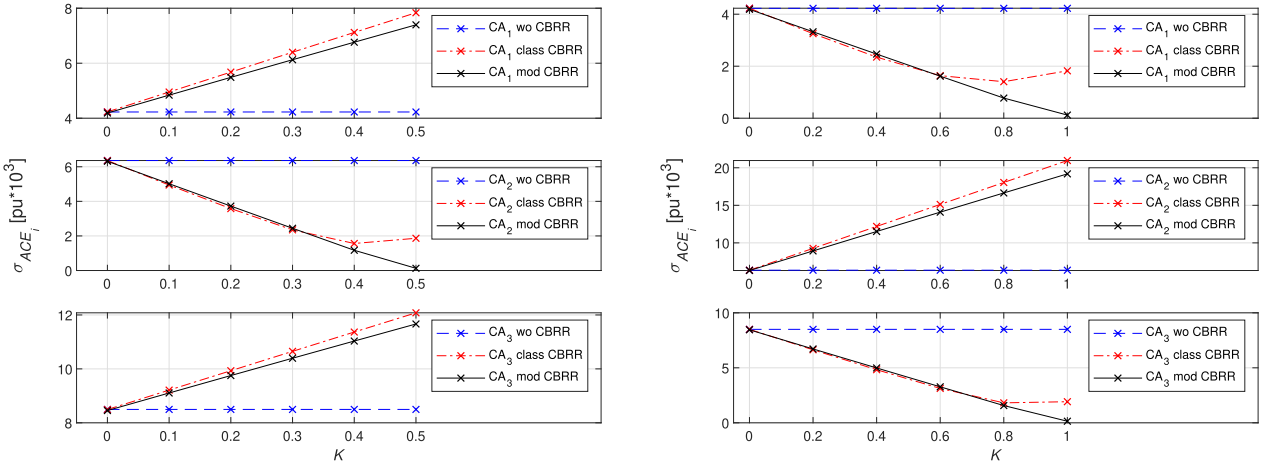

FIGURE 12. Values of σ_{ACE_i} for Case 1 (left) and Case 2 (right) in relation to K.

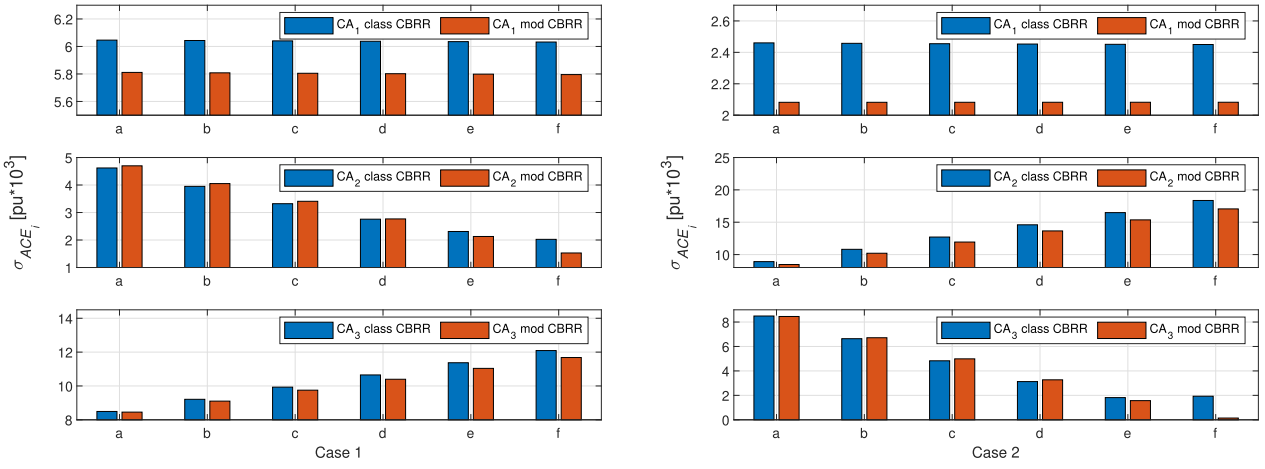

FIGURE 13. Average values of σ_{ACE_i} for Cases 1 a–f (left) and Cases 2 a–f (right).

of SGs inherently counteracts the load imbalances and thus limits the RoCoF. However, it becomes relevant in the case of significant load-generation imbalances, when larger RoCoF values can be observed due to the low system inertia caused by the high penetration of non-synchronously connected generation systems. Therefore, the Mean Value of the RoCoF_i, denoted as μ_{RoCoF_i}, is evaluated. The calculation is performed separately for positive and negative values, each of which is,

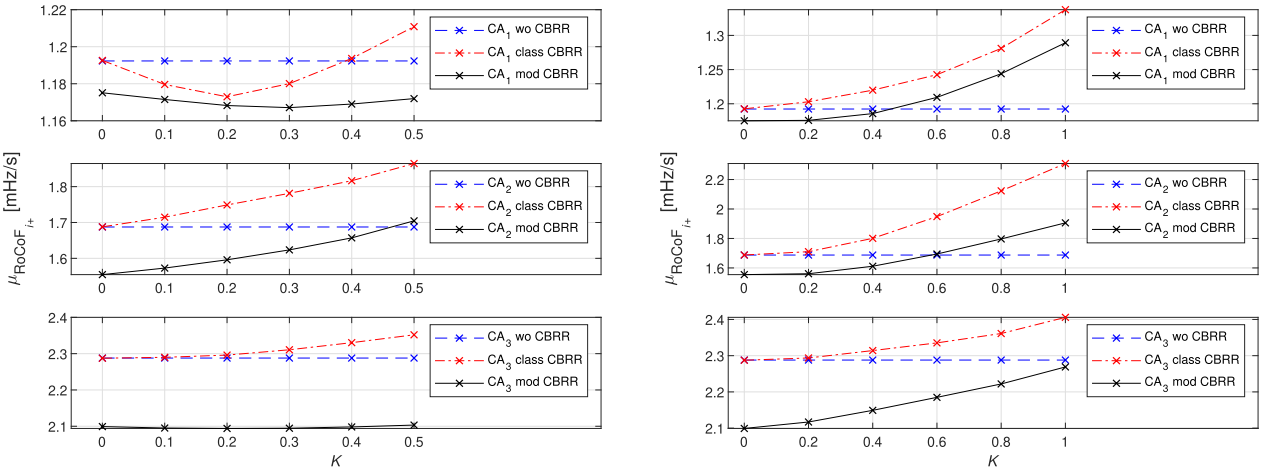

FIGURE 14. Values of $\mu_{\mathrm{RoCoF}_{i+}}$ for Case 1 (left) and Case 2 (right) in relation to K.

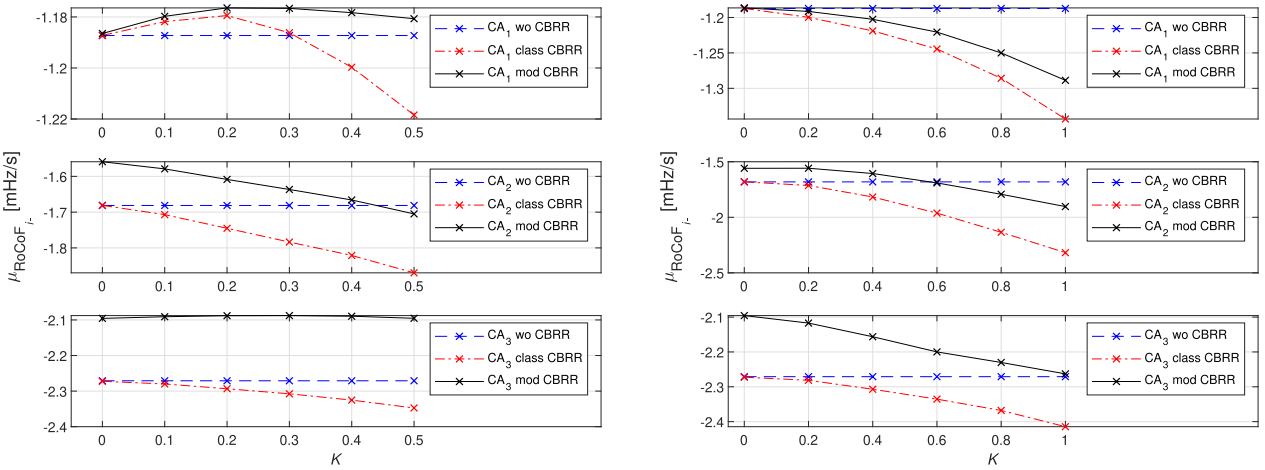

FIGURE 15. Values of $\mu_{\mathrm{RoCoF}_{i-}}$ for Case 1 (left) and Case 2 (right) in relation to K.

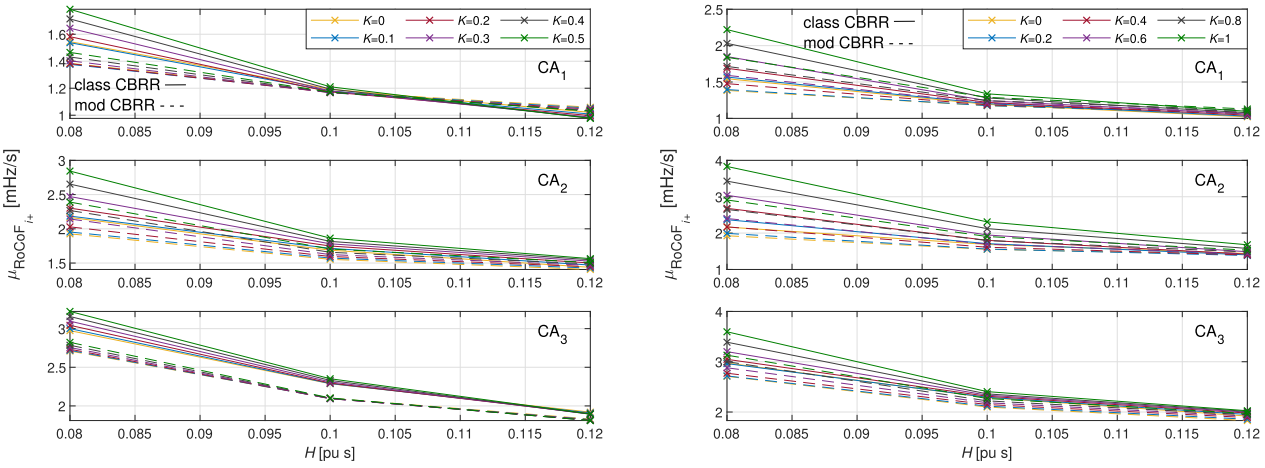

FIGURE 16. Values of $\mu_{\mathrm{RoCoF}_{i+}}$ for Case 1 (left) and Case 2 (right) in relation to H and different values of K.

respectively, denoted as $\mu_{\mathrm{RoCoF}_{i+}}$ and $\mu_{\mathrm{RoCoF}_{i-}}$. In addition, $\mu_{\mathrm{RoCoF}_{i+}}$ and $\mu_{\mathrm{RoCoF}_{i-}}$ are also evaluated for different values of the inertia time constant H and activation factor K.

The results of $\mu_{\mathrm{RoCoF}_{i+}}$ and $\mu_{\mathrm{RoCoF}_{i-}}$ are shown in Fig. 14 and Fig. 15 left for Case 1 and right for Case 2. In both Case 1 and Case 2 the classic CBRR increased $|\mu_{\mathrm{RoCoF}_{i+}}|$

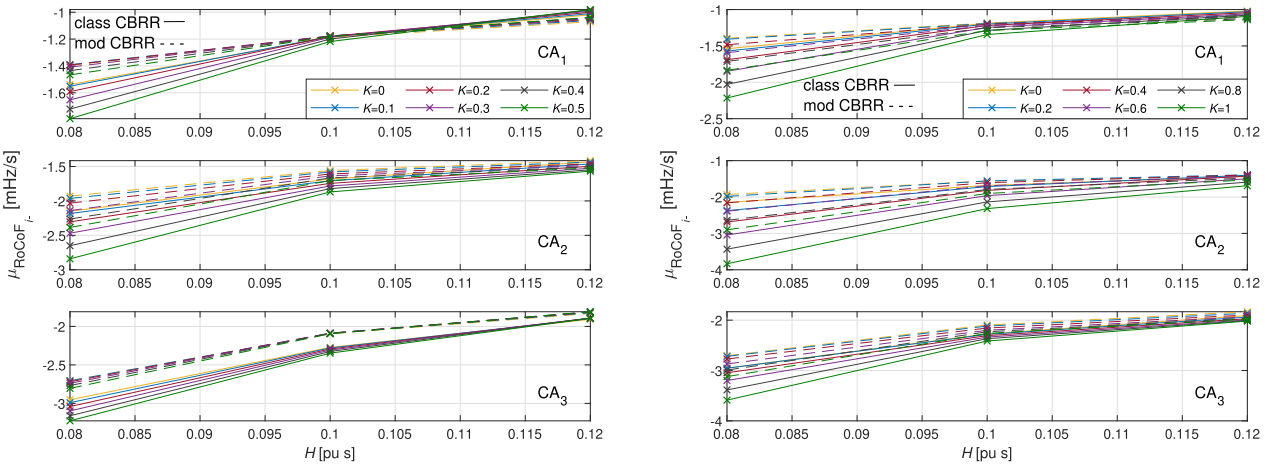

FIGURE 17. Values of $\mu_{\mathrm{RoCoF}_{i-}}$ for Case 1 (left) and Case 2 (right) in relation to H and different values of K.

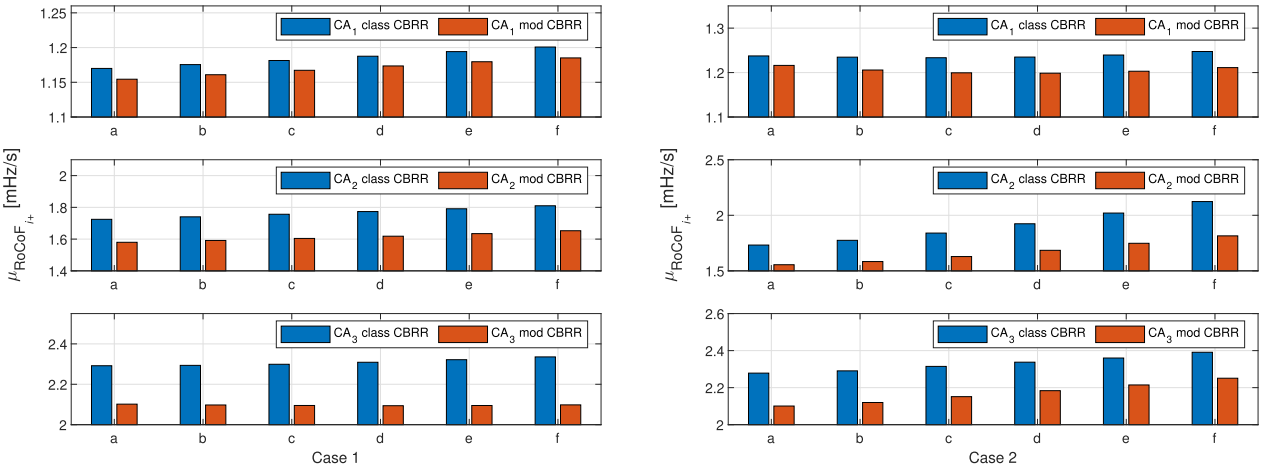

FIGURE 18. Average values of $\mu_{\mathrm{RoCoF}_{i+}}$ for Cases 1 a–f (left) and Cases 2 a–f (right).

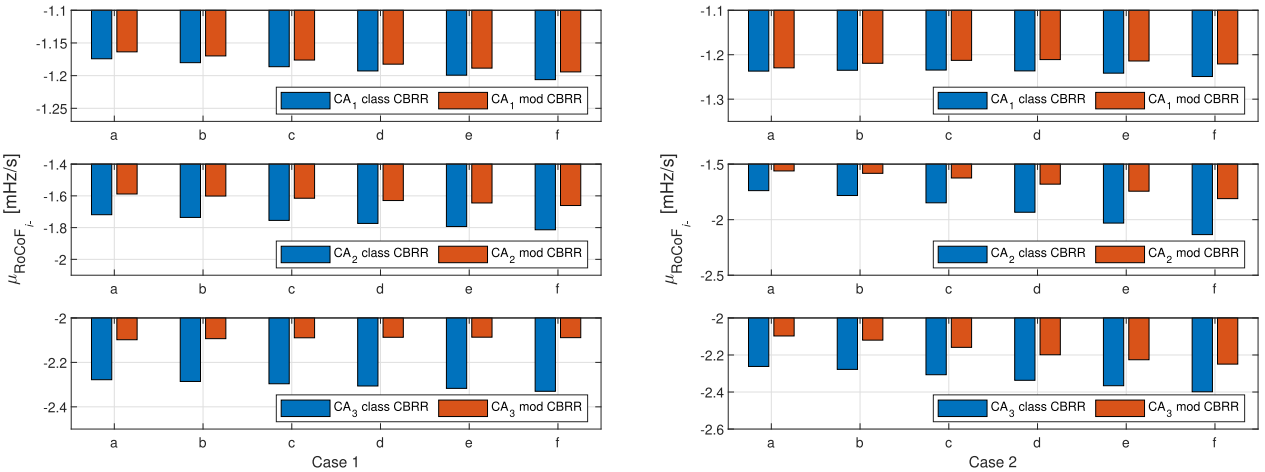

FIGURE 19. Average values of $\mu_{\mathrm{RoCoF}_{i-}}$ for Cases 1 a–f (left) and Cases 2 a–f (right).

and $|\mu_{\mathrm{RoCoF}_{i-}}|$ in all three CAs with the increase of K. The modified CBRR reduced $|\mu_{\mathrm{RoCoF}_{i+}}|$ and $|\mu_{\mathrm{RoCoF}_{i-}}|$ in all three CAs compared to the system with the classic CBRR and in some cases also compared to the system without the CBRR.

The results of $\mu_{\mathrm{RoCoF}_{i+}}$ and $\mu_{\mathrm{RoCoF}_{i-}}$ for different values of H are shown in Fig. 16 and Fig. 17 left for Case 1 and right for Case 2. The value of $|\mu_{\mathrm{RoCoF}_{i+}}|$ and $|\mu_{\mathrm{RoCoF}_{i-}}|$ is reduced with the increase of H, whereas it is increased with

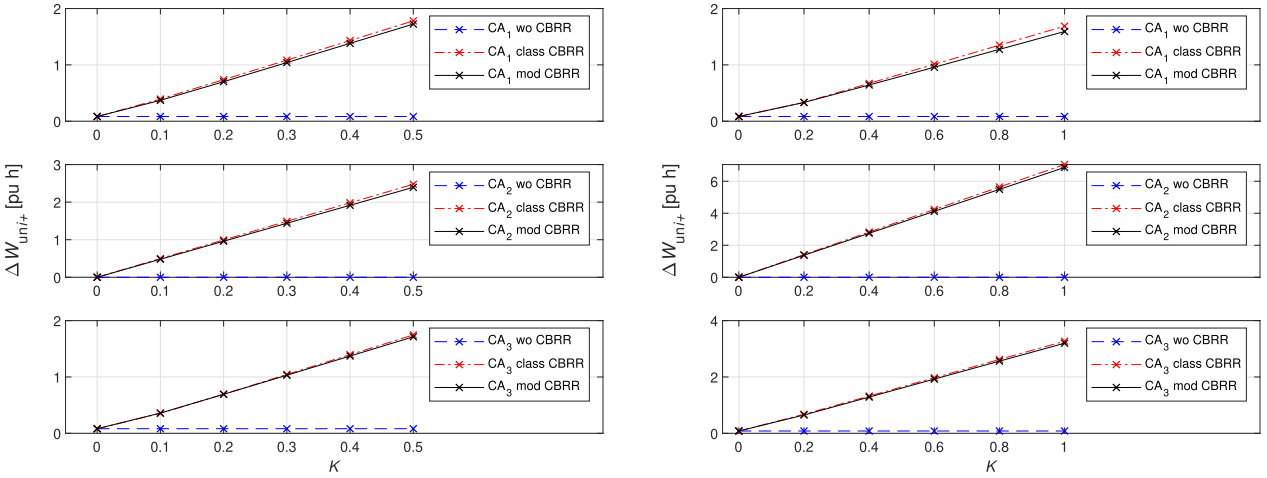

FIGURE 20. Values of ΔW_{uni+} for Case 1 (left) and Case 2 (right) in relation to K.

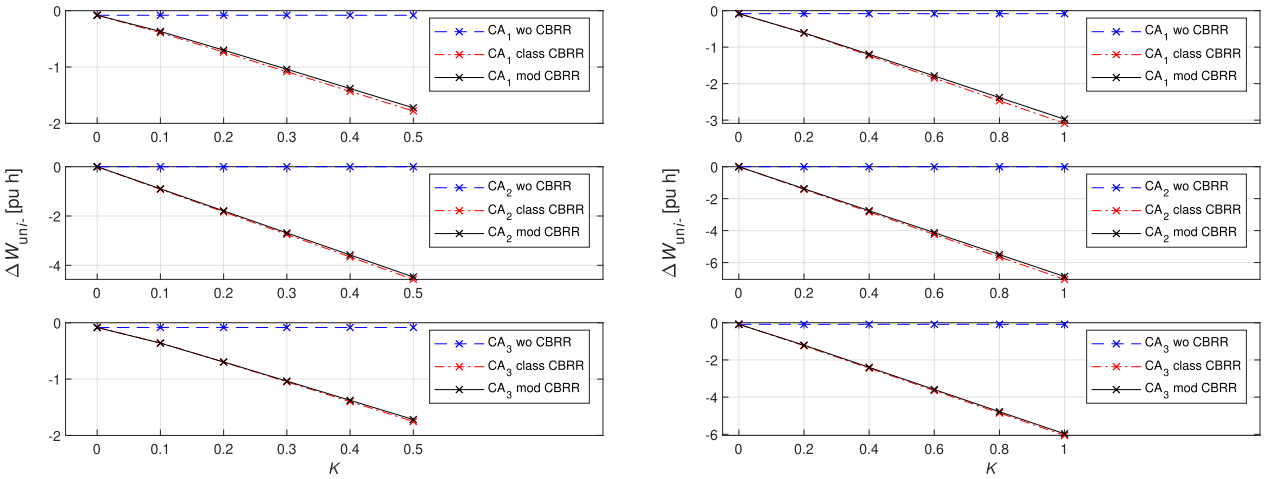

FIGURE 21. Values of ΔW_{uni-} for Case 1 (left) and Case 2 (right) in relation to K.

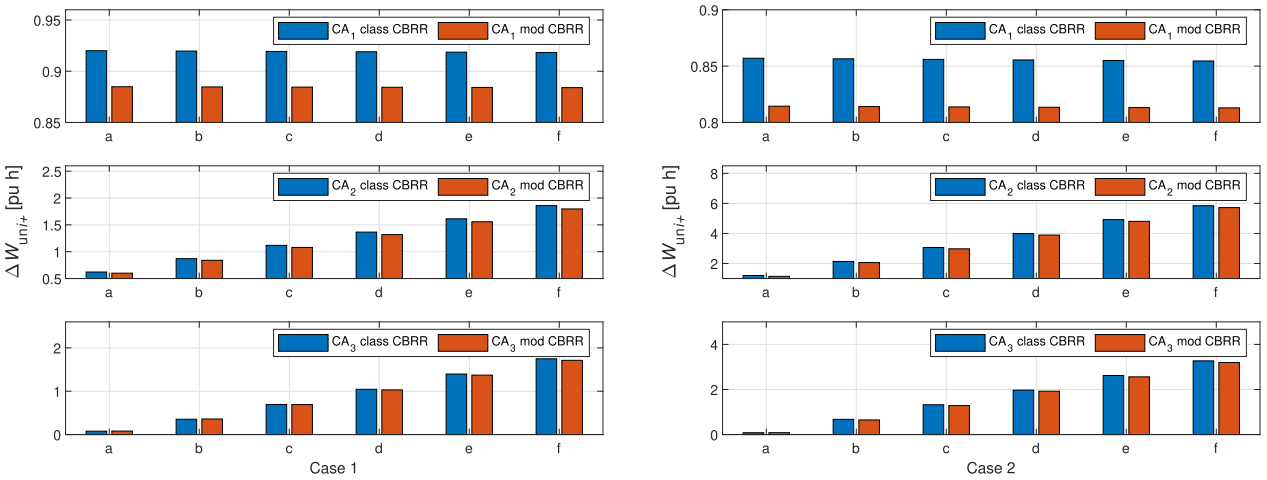

FIGURE 22. Average values of ΔW_{uni+} for Cases 1 a–f (left) and Cases 2 a–f (right).

the increase of K. However, the impact of H in combination with K is reduced on $|\mu_{\mathrm{RoCoF}_{i+}}|$ and $|\mu_{\mathrm{RoCoF}_{i-}}|$ when using the modified CBRR.

Figs. 18 and 19 show the results of an average value of $\mu_{\mathrm{RoCoF}_{i+}}$ and $\mu_{\mathrm{RoCoF}_{i-}}$, left for Cases 1 a–f and right for Cases 2 a–f. In all cases the modified CBRR reduced

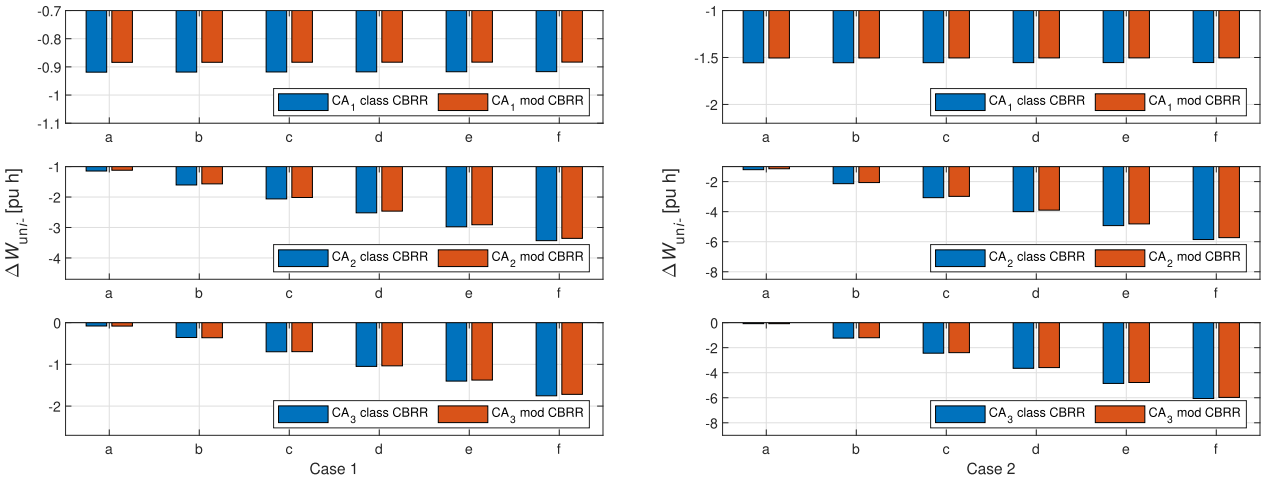

FIGURE 23. Average values of ΔW_{uni-} for Cases 1 a–f (left) and Cases 2 a–f (right).

$|\mu_{\mathrm{RoCoF}_{i+}}|$ and $|\mu_{\mathrm{RoCoF}_{i-}}|$ in all three CAs in comparison to the classic CBRR.

C. UNINTENDED EXCHANGE OF ENERGY

According to [19] this is the difference between scheduled exchanges and measured physical flows of electrical energy between TSOs. In addition to the interchange power variation, the correction power should also be taken into account. Thus, the unintended exchange of energy is calculated as

$$\Delta W_{\mathrm{uni}} = \Delta W_i - W_{\mathrm{cori}} = \int_0^t (\Delta P_i - P_{\mathrm{cori}})dt \qquad (29)$$

for the observed time period. The calculation is performed separately for positive and negative values, each of which is, respectively, denoted as $\Delta W_{\mathrm{uni}+}$ and $\Delta W_{\mathrm{uni}-}$. Note that 15-minute averages, as defined in [15], of the discussed variables were taken into account.

The results of $\Delta W_{\mathrm{uni}+}$ and $\Delta W_{\mathrm{uni}-}$ are shown in Fig. 20 and Fig. 21 left for Case 1 and right for Case 2. In both cases the classic CBRR increased the value of $|\Delta W_{\mathrm{uni}+}|$ and $|\Delta W_{\mathrm{uni}-}|$ in all three CAs with the increase of K. The modified CBRR reduced the value of $|\Delta W_{\mathrm{uni}+}|$ and $|\Delta W_{\mathrm{uni}-}|$ in all three CAs compared to the system with the classic CBRR. The reduction was in the range 2–3.3%.

Figs. 22 and 23 show the results of an average value of $\Delta W_{\mathrm{uni}+}$ and $\Delta W_{\mathrm{uni}-}$, left for Cases 1 a–f and right for Cases 2 a–f. In all cases the modified CBRR reduced $|\Delta W_{\mathrm{uni}+}|$ and $|\Delta W_{\mathrm{uni}-}|$ in all three CAs in comparison to the classic CBRR.

D. DEMAND POWER

The demand power of the i-th CA determines the maximum activation power for the i-th CA between the participating CAs with the same sign of ACE_i'. The demand power $P_{\mathrm{d}i}$ is calculated with (6) for the classic CBRR, while it is calculated with (12) for the modified CBRR. The calculations are performed separately for positive and negative values, each of which is, respectively, denoted as $P_{\mathrm{d}i+}$ and $P_{\mathrm{d}i-}$. Note that 15-minute averages, as defined in [15], of the discussed variables have been taken into account.

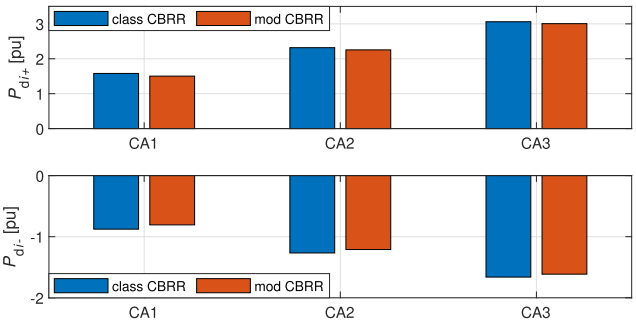

FIGURE 24. Values of P_{di+} and P_{di-}.

The results of $P_{\mathrm{d}i+}$ and $P_{\mathrm{d}i-}$ are shown in Fig. 24. Note that K does not affect $P_{\mathrm{d}i}$. Consequently, the values of $P_{\mathrm{d}i}$ for Case 1, Case 2, Cases 1 a–f and Cases 2 a–f are the same. It is clear that the modified CBRR reduces the values of $|P_{\mathrm{d}i+}|$ and $|P_{\mathrm{d}i-}|$ in all three CAs. The reduction for $|P_{\mathrm{d}i+}|$ is approximately 3.9%, while the reduction for $|P_{\mathrm{d}i-}|$ is approximately 2.5% in all three CAs.

VI. CONCLUSION

In this paper, a thorough analysis of CBRR activation was performed. It is clear that for a two-CA system the classic CBRR leads to reduced damping of the dominant eigenvalues, which negatively impacts the entire power system. Furthermore, using the classic CBRR, the impact of a tie-line parameter, inertia time constant, droop characteristic and frequency-bias coefficient on the system's eigenvalues did not change significantly. The proposed, i.e., modified CBRR, has no impact on the system's eigenvalues, thus inherently maintaining the system's eigendynamics.

Thorough dynamic simulations of a three-CA test system with the classic and modified CBRR were performed to evaluate the impact of the classic and modified CBRR on

the provision of LFC. The results of the random load variations confirmed that the classic CBRR impacts the frequency responses of participating CAs. The classic CBRR reduces the frequency deviations in the CAs where the activation is performed, while the modified CBRR reduces the frequency deviations in all the CAs. The classic CBRR increases the ACE deviations in the CAs where activation is performed, while the modified CBRR reduces the ACE deviations. The classic CBRR usually degrades the RoCoF in all the CAs, while the modified CBRR always improves the RoCoF. Moreover, the impact of the inertia time constant on the RoCoF is reduced with the modified CBRR. Due to the reduced unintended exchange of energy and demand power in all the CAs, positive financial effects can be expected when using the modified CBRR.

Future work should focus on the dynamic dimensioning of the CBRR. It was shown that CBRR activation reduces the overall use of regulating reserves, which is not taken into account in the reserve dimensioning. In this way, a possible over-sizing of the regulating reserves could be reduced.

REFERENCES

[1] J. Wu, J. Wen, H. Sun, and S. Cheng, "Feasibility study of segmenting large power system interconnections with AC link using energy storage technology," *IEEE Trans. Power Syst.*, vol. 27, no. 3, pp. 1245–1252, Aug. 2012.

[2] Q. Zhou and J. W. Bialek, "Approximate model of European interconnected system as a benchmark system to study effects of cross-border trades," *IEEE Trans. Power Syst.*, vol. 20, no. 2, pp. 782–788, May 2005.

[3] A. Ahmadi-Khatir, A. J. Conejo, and R. Cherkaoui, "Multi-area energy and reserve dispatch under wind uncertainty and equipment failures," *IEEE Trans. Power Syst.*, vol. 28, no. 4, pp. 4373–4383, Nov. 2013.

[4] J. W. Bialek, S. Ziemianek, and R. Wallace, "A methodology for allocating transmission losses due to cross-border trades," *IEEE Trans. Power Syst.*, vol. 19, no. 3, pp. 1255–1262, Aug. 2004.

[5] T. Strasser, F. Andren, J. Kathan, C. Cecati, C. Buccella, P. Siano, P. Leitao, G. Zhabelova, V. Vyatkin, P. Vrba, and V. Marik, "A review of architectures and concepts for intelligence in future electric energy systems," *IEEE Trans. Ind. Electron.*, vol. 62, no. 4, pp. 2424–2438, Apr. 2015.

[6] F. Blaabjerg, R. Teodorescu, M. Liserre, and A. V. Timbus, "Overview of control and grid synchronization for distributed power generation systems," *IEEE Trans. Ind. Electron.*, vol. 53, no. 5, pp. 1398–1409, Oct. 2006.

[7] D. E. Olivares, A. Mehrizi-Sani, A. H. Etemadi, C. A. Cañizares, R. Iravani, M. Kazerani, A. H. Hajimiragha, O. Gomis-Bellmunt, M. Saeedifard, R. Palma-Behnke, G. A. Jiménez-Estévez, and N. D. Hatziargyriou, "Trends in microgrid control," *IEEE Trans. Smart Grid*, vol. 5, no. 4, pp. 1905–1919, Jul. 2014.

[8] Imdadullah, S. M. Amrr, M. S. J. Asghar, I. Ashraf, and M. Meraj, "A comprehensive review of power flow controllers in interconnected power system networks," *IEEE Access*, vol. 8, pp. 18036–18063, Jan. 2020.

[9] ENTSO-E, Brussels, Belgium. (Nov. 2017). *Explanatory Document to all TSOs' Proposal for the Implementation Framework for a European Platform for the Exchange of Balancing Energy From Frequency Restoration Reserves With Automatic Activation in Accordance With Article 21 of Commission Regulation (EU) 2017/2195 of 23 November 2017 Establishing a Guideline on Electricity Balancing*. [Online]. Available: https://consultations.entsoe.eu/markets/afrr_implementation_framework/supporting_documents/20180426_aFRRIF_Explanatory_document.pdf

[10] ENTSO-E, Brussels, Belgium. (Nov. 2017). *Consultation on the Design of the Platform for Automatic Frequency Restoration Reserve (aFRR) of PICASSO Region*. [Online]. Available: https://eepublicdownloads.blob.core.windows.net/public-cdn-container/clean-documents/Network

[11] ENTSO-E, Brussels, Belgium. (May 2012). *Operational Reserve Ad Hoc Team Report*. [Online]. Available: https://entsoe.eu/resources/network-codes/loadfrequency-control-reserves/

[12] P. Kundur, *Power System Stability and Control*. New York, NY, USA: McGraw-Hill, 1994.

[13] Ibraheem, P. Kumar, and D. P. Kothari, "Recent philosophies of automatic generation control strategies in power systems," *IEEE Trans. Power Syst.*, vol. 20, no. 1, pp. 346–357, Feb. 2005.

[14] H. Bevrani, *Robust Power System Frequency Control*. New York, NY, USA: Springer, 2009.

[15] *Establishing a Guideline on Electricity Transmission System Operation*, Standard 2017/1485, Commission Regulation (EU), Aug. 2017. [Online]. Available: https://eur-lex.europa.eu/legal-content/EN/TXT/PDF/?uri=CELEX:32017R1485&from=EN

[16] P. Zolotarev, M. Gökeler, M. Kuring, H. Neumann, and E. M. Kurscheid, "Grid control cooperation–a framework for technical and economical crossborder optimization for load-frequency control," in *Proc. 44th Int. Conf. Large High Voltage Electr. Sys. (CIGRE)*, Paris, France, Aug. 2012, pp. 1–13.

[17] A. Cronenberg, N. Seeger, and S. Willemsen, "Integration of France into the international grid control cooperation," in *Proc. IEEE Int. Energy Conf. (ENERGYCON)*, Leuven, Belgium, Apr. 2016, pp. 1–6.

[18] ENTSO-E, Brussels, Belgium. (Sep. 2016). *Stakeholder Document for the Principles of IGCC*. [Online]. Available: https://eepublicdownloads.blob.core.windows.net/public-cdn-container/clean-documents/Network

[19] *Establishing a Guideline on Electricity Balancing*, Standard 2017/2195, Commission Regulation (EU), Nov. 2017. [Online]. Available: https://eur-lex.europa.eu/legal-content/EN/TXT/PDF/?uri=CELEX:32017R2195&from=EN

[20] Explore. (Oct. 2016). *Target Model for Exchange of Frequency Restoration Reserves*. [Online]. Available: https://erranet.org/wp-content/uploads/2017/02/20161021_EXPLORE_FRR_TARGET_MODEL.pdf

[21] ENTSO-E, Brussels, Belgium. (Jun. 2013). *Supporting Document for the Network Code on Load-Frequency Control and Reserves*. [Online]. Available: https://www.acer.europa.eu/Official_documents/Acts_of_the_Agency/Annexes/ENTSO-E

[22] H. H. Alhelou, M. E. H. Golshan, R. Zamani, E. H. Forushani, and P. Siano, "Challenges and opportunities of load frequency control in conventional, modern and future smart power systems: A comprehensive review," *Energies*, vol. 11, no. 10, pp. 1–35, Sep. 2018.

[23] R. A. C. van der Veen, A. Abbasy, and R. A. Hakvoort, "Analysis of the impact of cross-border balancing arrangements for Northern Europe," in *Proc. 8th Int. Conf. Eur. Energy Market (EEM)*, Zagreb, Croatia, May 2011, pp. 653–658.

[24] L. Vandezande, L. Meeus, M. Saguan, J.-M. Glachant, and R. Belmans, "Implementation of cross-border balancing in Europe," in *Proc. 1st Int. Conf. Infrastruct. Syst. Services, Building Netw. Brighter Future (INFRA)*, Rotterdam, The Netherlands, 2008, pp. 1–6.

[25] F. M. Baldursson, E. Lazarczyk, M. Ovaere, and S. Proost, "Multi-TSO system reliability: Cross-border balancing," in *Proc. IEEE Int. Energy Conf. (ENERGYCON)*, Leuven, Belgium, Apr. 2016, pp. 1–6.

[26] I. Avramiotis-Falireas, H. Qu, F. Abbaspourtorbati, and M. Zima, "The importance of accurate transmission system model for cross-border exchange of balancing energy," in *Proc. 13th Int. Conf. Eur. Energy Market (EEM)*, Porto, Portugal, Jun. 2016, pp. 1–4.

[27] I. G. Marneris, C. G. Roumkos, and P. N. Biskas, "Towards balancing market integration: Conversion process for balancing energy offers of central-dispatch systems," *IEEE Trans. Power Syst.*, vol. 35, no. 1, pp. 293–303, Jan. 2020.

[28] J. D. Sprey, P. Schultheis, and A. Moser, "Dynamic dimensioning of balancing reserve," in *Proc. 14th Int. Conf. Eur. Energy Market (EEM)*, Dresden, Germany, Jun. 2017, pp. 1–5.

[29] M. Topler, J. Ritonja, and B. Polajžer, "The impact of the imbalance netting process on power system dynamics," *Energies*, vol. 12, no. 24, pp. 1–18, Dec. 2019.

[30] M. Topler, J. Ritonja, R. Brezovnik, and B. Polajzer, "Impact of imbalance netting cooperation on frequency quality and provision of load-frequency control," in *Proc. IEEE Int. Conf. Environ. Electr. Eng. IEEE Ind. Commercial Power Syst. Eur. (EEEIC / I&CPS Europe)*, Genoa, Italy, Jun. 2019, pp. 1–6.

[31] O. Elgerd and C. Fosha, "Optimum megawatt-frequency control of multi-area electric energy systems," *IEEE Trans. Power App. Syst.*, vol. PAS-89, no. 4, pp. 556–563, Apr. 1970.

[32] P. Vorobev, D. M. Greenwood, J. H. Bell, J. W. Bialek, P. C. Taylor, and K. Turitsyn, "Deadbands, droop, and inertia impact on power system frequency distribution," *IEEE Trans. Power Syst.*, vol. 34, no. 4, pp. 3098–3108, Jul. 2019.

[33] P. Kundur, J. Paserba, V. Ajjarapu, G. Andersson, A. Bose, C. Canizares, N. Hatziargyriou, D. Hill, A. Stankovic, C. Taylor, T. Van Cutsem, and V. Vittal, "Definition and classification of power system stability IEEE/CIGRE joint task force on stability terms and definitions," *IEEE Trans. Power Syst.*, vol. 19, no. 3, pp. 1387–1401, Aug. 2004.
[34] P. M. Anderson and M. Mirheydar, "A low-order system frequency response model," *IEEE Trans. Power Syst.*, vol. 5, no. 3, pp. 720–729, Aug. 1990.
[35] E. Janecek, V. Cerny, A. Fialova, and J. Fantik, "A new approach to modelling of electricity transmission system operation," in *Proc. IEEE PES Power Syst. Conf. Expo.*, Atlanta, GA, USA, Oct./ Nov. 2006, pp. 1429–1434.
[36] NERC. (Nov. 2012). *Frequency Response Standard, Background Document*. [Online]. Available: https://www.nerc.com/pa/Stand/Project
[37] ENTSO-E, Brussels, Belgium. (Jun. 2017). *Frequency Quality, Phase 2*. [Online]. Available: https://www.statnett.no/globalassets/for-aktorer-i-kraftsystemet/utvikling-av-kraftsystemet/nordisk-frekvensstabilitet/frequency-quality-phase-2-v1.2.pdf
[38] ENTSO-E, Brussels, Belgium. (Jun. 2013). *Network Code on Load-Frequency Control and Reserves*. [Online]. Available: https://www.acer.europa.eu/Official_documents/Acts_of_the_Agency/Annexes/The
[39] ENTSO-E, Brussels, Belgium. (Mar. 2017). *Rate of Change of Frequency (ROCOF) Withstand Capability*. [Online]. Available: https://eepublicdownloads.blob.core.windows.net/public-cdn-container/clean-documents/Network

MARCEL TOPLER (Graduate Student Member, IEEE) received the M.Eng. degree in electrical engineering from the Faculty of Electrical Engineering and Computer Science, University of Maribor, Maribor, Slovenia, in 2017. Since 2017, he has been an Assistant Professor of Electrical Engineering with the Faculty of Electrical Engineering and Computer Science, University of Maribor. His current research interests include power system control and electrical machines.

JOŽEF RITONJA (Member, IEEE) received the B.S., M.S., and Ph.D. degrees in electrical engineering from the Faculty of Electrical Engineering and Computer Science, University of Maribor, Maribor, Slovenia, in 1986, 1989, and 1996, respectively. Since 1987, he has been with the Faculty of Electrical Engineering and Computer Science, University of Maribor. His research interests include control theory, electrical machines, and power systems.

BOŠTJAN POLAJŽER (Member, IEEE) received the B.Sc. and Ph.D. degrees in electrical engineering from the Faculty of Electrical Engineering and Computer Science, University of Maribor, Maribor, Slovenia, in 1997, and 2002, respectively. Since 1998, he has been with the Faculty of Electrical Engineering and Computer Science, University of Maribor, where he has been an Associate Professor, since 2010. In 2000, he was a Visiting Scholar with the Catholic University Leuven, Leuven, Belgium, and with the Graz University of Technology, Graz, Austria, in 2019. His research interests include electrical machines and devices, power quality, and power-system protection and control.